Contents lists available at ScienceDirect

ISPRS Journal of Photogrammetry and Remote Sensing

journal homepage: www.elsevier.com/locate/isprsjprs

Individual tree crown delineation in a highly diverse tropical forest using very high resolution satellite images

Fabien Hubert Wagner[a,*], Matheus Pinheiro Ferreira[a,f], Alber Sanchez[a], Mayumi C.M. Hirye[a], Maciel Zortea[b], Emanuel Gloor[c], Oliver L. Phillips[c], Carlos Roberto de Souza Filho[d], Yosio Edemir Shimabukuro[a], Luiz E.O.C. Aragão[a,e]

[a] *Remote Sensing Division, National Institute for Space Research – INPE, São José dos Campos, 12227-010 SP, Brazil*
[b] *IBM Research Brazil, Avenida Pasteur 138, 22290-240 Rio de Janeiro, RJ, Brazil*
[c] *Ecology and Global Change, School of Geography, University of Leeds, LS2 9JT Leeds, UK*
[d] *Geosciences Institute, University of Campinas, R. João Pandiá Calógeras 51, 13083-870 Campinas, SP, Brazil*
[e] *College of Life and Environmental Sciences, University of Exeter, Exeter EX4 4RJ, United Kingdom*
[f] *Cartography Engineering Section, Military Institute of Engineering - IME, Praça Gen. Tibúrcio 80, 22290-270 Rio de Janeiro, RJ, Brazil*

A R T I C L E   I N F O

A B S T R A C T

Mapping tropical tree species at landscape scales to provide information for ecologists and forest managers is a new challenge for the remote sensing community. For this purpose, detection and delineation of individual tree crowns (ITCs) is a prerequisite. Here, we present a new method of automatic tree crown delineation based only on very high resolution images from WorldView-2 satellite and apply it to a region of the Atlantic rain forest with highly heterogeneous tropical canopy cover – the Santa Genebra forest reserve in Brazil. The method works in successive steps that involve pre-processing, selection of forested pixels, enhancement of borders, detection of pixels in the crown borders, correction of shade in large trees and, finally, segmentation of the tree crowns. Principally, the method uses four techniques: rolling ball algorithm and mathematical morphological operations to enhance the crown borders and ease the extraction of tree crowns; bimodal distribution parameters estimations to identify the shaded pixels in the gaps, borders, and crowns; and focal statistics for the analysis of neighbouring pixels. Crown detection is validated by comparing the delineated ITCs with a sample of ITCs delineated manually by visual interpretation. In addition, to test if the spectra of individual species are conserved in the automatic delineated crowns, we compare the accuracy of species prediction with automatic and manual delineated crowns with known species. We find that our method permits detection of up to 80% of ITCs. The seven species with over 10 crowns identified in the field were mapped with reasonable accuracy (30.5–96%) given that only WorldView-2 bands and texture features were used. Similar classification accuracies were obtained using both automatic and manual delineation, thereby confirming that species' spectral responses are preserved in the automatic method and thus permitting the recognition of species at the landscape scale. Our method might support tropical forest applications, such as mapping species and canopy characteristics at the landscape scale.

1. Introduction

The world's forests play key roles in maintaining environmental processes, such as the water cycle, soil conservation, carbon sequestration and habitat protection (FAO, 2016). In particular, tropical forests host the overwhelming proportion of global tree diversity, with as many as 53,000 tree species or more, in contrast to only 124 across temperate Europe (Slik et al., 2015), and provide critical ecosystem services to mitigate climate change. One of the most documented roles of tropical forests is their potential to act as a carbon sink, which accounts for approximately half (1.19 ± 0.41 PgC yr^{-1}) of the global sink of established forests (Pan et al., 2011; Baccini et al., 2012). This carbon sink service is significant, for example, the mature Amazon forests alone mitigated the carbon emissions of all the Amazon countries between 1980 and 2010 (Phillips and Brienen, 2017). Due to the importance of these forests, it is crucial to build a reliable forest inventory at the individual tree level – with information on key parameters such as tree species, tree diameter and height, crown size and

---

location – for a range of scientific and applied purposes including resource management, biodiversity assessment, ecosystem services assessment and conservation.

Conventional field inventory of individual trees is a challenging task in tropical environments in terms of time, effort and cost. Consequently, tree ecological field surveys in tropical forests typically cover areas of ~1 ha (Mitchard et al., 2014), with a very few up to 50 ha, such as Barro Colorado Island (BCI, Panama) or Pasoh (Malaysia) (Condit et al., 1999). Consequently, the total area of the field plots surveyed since the 1950s in the Amazon forests likely represents less than 0.0001% of the total area of this biome (Saatchi et al., 2015), and for the Atlantic forest, an estimated 0.01% of the total area has been surveyed (de Lima et al., 2015). A re-census of the tropical forest permanent plots is typically made every 1–5 years, with a mean time of ~3 years (Mitchard et al., 2014). While mortality rates have increased across the Amazon forest plots (Phillips et al., 2009; Brienen et al., 2015), the time between the censuses hinders the analysis of the potential annual or intra-annual climate drivers of mortality.

Thus, forest inventory at the landscape scale remains a major challenge, and one likely to be best tackled by a combination of remote sensing information and ground truth. In this context, airborne and satellite sensors can now acquire images with sub-metric spatial resolution, thereby enabling the detection of individual tree crowns (ITCs). They also provide spectral and structural information which can be used to identify canopy species, extract tree metrics such as crown size, and estimate stand characteristics such as canopy structure or biomass (Palace et al., 2008; Ferreira et al., 2016; Singh et al., 2015; Laurin et al., 2014). Furthermore, frequent satellite image acquisitions can enable annual or inter-annual surveys.

The detection and delineation of ITCs is a prerequisite for individual tree inventory over large spatial extents (Clark et al., 2005). Such ITCs can be used in object-oriented image analysis and provide information such as tree count, location, crown size, distance between individuals, and tree species. Accurate ITC delineation improves spectral signature characterization (by reducing the number of pixels outside of the actual crown) and is a requirement in majority voting approaches for spectral species recognition (Fassnacht et al., 2016). Another advantage of this approach is that additional attributes can be obtained for each object, here defined as tree crown, such as reflectance value distributions or textural information. Information at the tree crown level can improve the classification of tree species (Clark et al., 2005; Feret and Asner, 2013; Warner et al., 2006; Fassnacht et al., 2016; Ferreira et al., 2016). In contrast, pixel-wise analysis, which does not require the identification of crowns, is unsuitable for individual tree inventory, but can be used to map whole stand characteristics such as species composition (Vaglio Laurin et al., 2014; Cho et al., 2015), canopy biochemical contents (Asner et al., 2017), biodiversity (Feret and Asner, 2014), species invasion (Amaral et al., 2015), and biomass (Laurin et al., 2014; Mutanga et al., 2012).

Advances in hyperspectral and Light detection and ranging (LiDAR) remote sensing imagery allow automatic and accurate ITC detection (mostly above 60% of the canopy trees), in both temperate and tropical forest ecosystems (Lee et al., 2016; Tochon et al., 2015; Ferreira et al., 2016; Singh et al., 2015; Dalponte et al., 2014; Feret and Asner, 2013). However, these methods are expensive due to data collection (mostly with a sensor mounted on an airborne platform) and are becoming increasingly complex and data demanding, thereby limiting their reproducibility (Tochon et al., 2015; Lee et al., 2016). In comparison to both field surveys and airborne campaigns, very high spatial resolution imagery acquired by satellite sensors is an affordable alternative (~30 US$ for one km^2 of WorldView-2 images) and users can access forest information with multispectral resolution. For example, WorldView-2 (WV-2) images provided to the users have 8 multispectral bands and one panchromatic band with a spatial resolution of 2 m and 0.5 m, respectively (DigitalGlobe, 2017). The WorldView-2 waveband combination is suitable for assessing vegetation characteristics that vary

between species and, hence, might be adequate for species discrimination in tropical forests (Cho et al., 2012, 2015; Latif et al., 2012; Heenkenda et al., 2014). WorldView-2 also offers a large archive, enabling users to select the images with the best angular characteristics for detecting ITCs and also providing them time series for the studied areas. The automatic delineation of tree crowns in tropical forests using only WV-2 images is theoretically feasible but remains as an open challenge due to the complexity of the canopy, that is, very dense vegetation, different crown sizes, overlapping tree crowns, and absence of clear boundaries between individuals (Latif et al., 2012; Feret and Asner, 2013).

The delineation of ITCs can be done manually or automatically. Manual crown delineation from images has been used in recent literature on tropical tree species recognition in small areas (Clark et al., 2005; Caughlin et al., 2016), but is not suitable to study areas above ~100 ha. Numerous algorithms exist for automatic delineation, but most of them have been developed for temperate forest stands (Ke and Quackenbush, 2011; Duncanson et al., 2014) and their application to deciduous and tropical forests has proven to be much more challenging, but not impossible (Feret and Asner, 2013; Bunting et al., 2009; Leckie et al., 2003; Ferreira et al., 2016; Warner et al., 2006). The automatic methods for ITC delineation from passive remote sensing assume that the tree crowns have the shape of a mountain, with bright peaks at the treetops and dark pixels at the border of the crown (Ke and Quackenbush, 2011). The methods of automatic ITC delineation can be classified into two groups, based on tree border (valley following, watershed segmentation) or based on the spectral characteristics (region growing, template matching) (reviewed in Ke and Quackenbush (2011)). While using the brightest point as the top of the trees is a reasonable approach in many temperate forests, particularly in coniferous stands, this is likely to be overly simplistic for tropical forest environments due to the variety of architectures and crown sizes exhibited. For example, for a large rounded crown, the bright pixels may appear not at the point of maximum height but rather on the border exposed to the Sun, while for flat crowns there could be no difference in brightness at all. On the other hand, identifying ITCs from the spectral signature has three major limitations in a tropical forest: (i) trees may be partially covered by lianas, thereby altering the spectral response of species (Kalacska et al., 2007), (ii) a tree can have new leaves only on a part of its crown, which results in markedly different spectral responses in the same crown (Lopes et al., 2016) and (iii) due to the diverse architecture and leaf characteristics of tropical trees, the intra-crown spectral variability among different species is also likely to be highly diverse (Ferreira et al., 2016). All these challenges make it difficult to select a single, unique forest-wide threshold for the spectrum-based methods for ITC detection, such as the region-growing algorithms (Culvenor, 2002; Erickson, 2004).

Based on these identified limitations in tropical forests, we explored a method of automatic tree crown delineation based only on border detection. Our main assumptions are that the border of trees contains more shade than the tree crowns, that the shade in the large tree crowns can be identified and corrected and that the resulting shade of the edge can be contrasted by numerical methods to enable the extraction of tree crowns. Our method belongs to the first group of methods to delineate ITCs, which is based on tree border identifications.

Species identification with remote sensing in tropical forests is a current topic, with less than 20 studies published before 2015 for this ecosystem (Fassnacht et al., 2016). WorldView-2 is amongst the promising very high resolution (VHR) multispectral satellite sensors for species identification. This sensor was successfully used to discriminate and map tree species in temperate forests (Immitzer et al., 2012; Waser et al., 2014), urban areas (Pu and Landry, 2012; Pu et al., 2015), mangrove areas (Heenkenda et al., 2014), forest plantations (Peerbhay et al., 2014) and sub-tropical forests (Cho et al., 2015). However, in these studies, species recognition is made at the pixel level and not at the crown level, thereby limiting the information for species

classification to pixel reflectance. For WorldView-2 images, accurate ITC delineation should improve tree species identification, as observed with remote sensed images from other sources (Clark et al., 2005; Ferreira et al., 2016; Dalponte et al., 2014; Fassnacht et al., 2016).

For complex ecosystems such as tropical forests, accurate ITC delineations might be used to extract not only pixel reflectance but also crown characteristics that are useful for species identification (Fassnacht et al., 2016). For example, in addition to the multispectral bands, WV-2 features a sub-metric panchromatic band that can be used to detect texture attributes of the tree crowns, which is related to crown-internal shadows, branching and foliage properties among species (Fassnacht et al., 2016). Furthermore, with the ITCs, the distribution of reflectances per crown or per species can be accessed. All this information on the optical properties of species at the crown level might improve classification accuracy. However, little is known yet about the utility of the optical properties (reflectance and texture) at the crown level for tree species mapping in tropical forests. Our assumption is that species can be discriminated in tropical forests with Worldview-2 image by using species classification based on ITCs.

The objectives of this work are (i) to provide a simple, automatic and reproducible method to detect and delineate canopy tree crowns in highly diverse tropical forests, taking advantage of commercial very high resolution WorldView-2 imagery and (ii) to test if the spectral signature of the species is conserved in the delineated crown, and, if so, produce forest inventory maps of seven selected tree species based on field and spectral data and automatic delineated tree crowns.

2. Materials

2.1. Study site

The study site is the *Santa Genebra* Forest Reserve, a remnant of the Atlantic Forest biome, located in the municipality of Campinas (São Paulo State - Brazil) and centered at 22°49′13.46″S and 47°06′38.47″W, as shown in Fig. 1. The elevation of the study area ranges from 580 to 610 m. The terrain consists of a relatively smooth relief with forest located on the higher elevation and occupying 85% of the reserve (Leito Filho and Morellato, 1995). The reserve comprises 237.6 ha of a well-preserved submontane semi-deciduous forest formation (Oliveira-Filho and Ratterf, 1995). The site receives approximately 1500 mm of precipitation per year and is subject to a dry season that lasts for 4–5 months between April and September, during which rainfall is less than 100 mm.month^{-1} (CRU TS3.21, 2014). The mean annual temperature is 20.5 °C and ranges from 11.0 to 28.5 °C. Floristic surveys performed in the area found ≈100 woody species within one hectare (Farah et al., 2014; Guaratini et al., 2008). The forest canopy is highly heterogeneous and comprises both deciduous and evergreen species (Farah et al., 2014).

2.2. WorldView-2 images and pre-processing

The WorldView-2 image (DigitalGlobe, Inc., USA) over the forest of *Santa Genebra* was acquired on 11 December 2014, under clear sky conditions and at an average off nadir view angle of 2.4°. The spatial resolution of the bands is 0.5 m for the panchromatic band (464–801 nm) and 2 m for the multispectral bands: Red (629–689 nm), Green (511–581 nm) and Blue (447–508 nm). The bands were scaled from raw image digital numbers (11 bit) to 0–255 (8 bit). The Red-Green-Blue (RGB) bands were then pan-sharpened, that is, merged with the high-resolution panchromatic image to create a single high-resolution RGB image at 0.5 m resolution. The RGB bands were pan-sharpened with the panchromatic band using the High Pass Filter Additive (HPFA) fusion technique (Gangkofner et al., 2008) provided by the GRASS GIS addon `i.fusion.hpf` (GRASS Development Team, 2017). For WorldView-2 images, the HPFA method has been recently shown to be among the best pan-sharpening algorithms for the conservation of spectral responses (Nikolakopoulos and Oikonomidis, 2015). We used GRASS GIS version 7.3.svn.

2.3. Field data

Individual Tree Crowns were manually delineated using the pan-sharpened WorldView-2 image and a previous ITC reference dataset for the study area (Ferreira et al., 2016). Only crowns that were clearly seen by visual interpretation were selected and manually delineated on the image. Then the selected trees were identified at the species level in the field with the aid of a GPS device coupled to an external antenna (Garmin 65CSx ©). The GPS accuracy during the field work was approximately 3 m. The presence of lianas over the crowns was carefully inspected to avoid liana-dominated trees. A total of 370 suitable ITCs were identified, corresponding to 34 species. Most of the located trees exhibited a large crown and a large diameter at breast height (DBH) with values ranging from 19 to 111 cm and with a mean of 58.7 cm (Ferreira et al., 2016) and thus could be easily found in the field. For classification purposes, we selected 7 species from among the 34 sampled, with more than 10 trees visited in the field, Table 1.
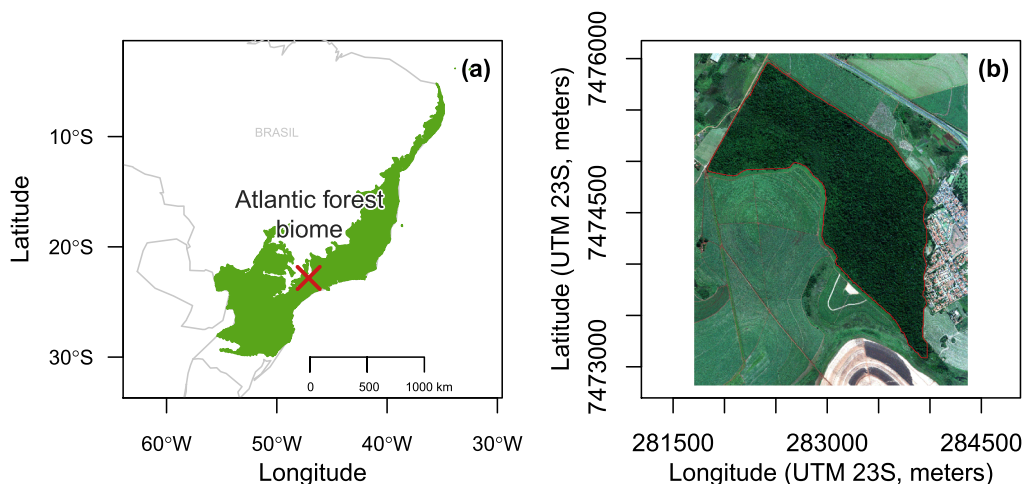

Fig. 1. Geographical locations of the Atlantic forest biome in green and of the forest of Santa Genebra in red (a); WorldView-2 image used in this study with the limits of the Santa Genebra forest in red (b). (For interpretation of the references to color in this figure legend, the reader is referred to the web version of this article.)

Table 1
Description of the trees with crowns manually delineated in the WV-2 image and identified in the field: species list, species code, number of ITCs, mean ITC size (pixels), minimum crown size (pixels), maximum crown size (pixels) and total pixels of the species.

Species	Code	ITCs	Mean crown size	Min crown size	Max crown size	Pixels
Aspidosperma polyneuron	AP	23	386	157	846	8888
Astronium graveolens	AG	56	363	78	1608	20,350
Cariniana legalis	CL	50	954	220	1980	47,719
Cecropia hololeuca	CH	54	117	5	272	6335
Croton piptocalyx	CP	63	252	46	624	15,895
Diatenopteryx sorbifolia	DS	18	83	33	136	1500
Hymenaea courbaril	HC	18	626	188	1640	11,270

3. Methods

3.1. Image processing algorithms

In our algorithm, we mainly used three methods to process the image, one statistical method based on the characteristics of the grayscale values distribution of the forest image to determine if a given pixel is in a tree or in a border, and two image processing algorithms: the rolling ball algorithm and mathematical morphological operation. These two latter algorithms have been used to enhance the tree border and ease the segmentation of the tree crowns. The details of these methods are provided below.

3.1.1. Estimation of bimodal distribution parameters

To determine if a pixel is in the shade or in a tree crown, our first approach is based on the grayscale values of the pixels. In our method, the grayscale scale images were produced by converting the RGB image to a hue, saturation, and lightness (HSL) image and keeping only the L channel. In all the following text, grayscale values refer to the value of the L channel. The distribution of the grayscale values of the forest image can be considered as a mixture distribution of two ecological features, Fig. 2. The first (blue distribution) is the natural variation of illuminated vegetation pixels in the tree crowns, while the second (red distribution) represents the variation of the shaded pixels in the forest gaps, similar to what is observed with height measured by LiDAR over tropical forests (Goulamoussène et al., 2017), see Fig. 6a. To determine the parameters of the two underlying normal distributions and their overlap, we used an Expectation-Maximization algorithm (EM algorithm) for mixtures of univariate normals (Benaglia et al., 2009). Then, different thresholds have been set depending on the purpose, that is, to eliminate or to keep dark pixels. This method has also been used on the distribution of distance to dark pixels. In the following text, we refer to the distribution with lower grayscale values as grayscale values in gaps and to the higher distribution as grayscale values in the forest. Details of the thresholds are provided in the algorithm description.

3.1.2. Rolling ball algorithm

The rolling ball algorithm (Stanley R Sternberg and CytoSystems Corporation, 1983; Kneen and Annegarn, 1996), Eqs. (1)–(4), is used to contrast images in order to enhance the shade of the tree crowns border and also to remove/extract objects in images, for example, to extract tree crowns above the minimum defined tree crown size. A local background value (the baseline, b_i, Eq. (3)) is determined for every pixel by averaging over a very large ball of radius r around the pixel, Fig. 3. This value can be subtracted from the original image to remove large spatial variation of the background intensities (the radius of the rolling ball is selection to be at least the size of the largest object).
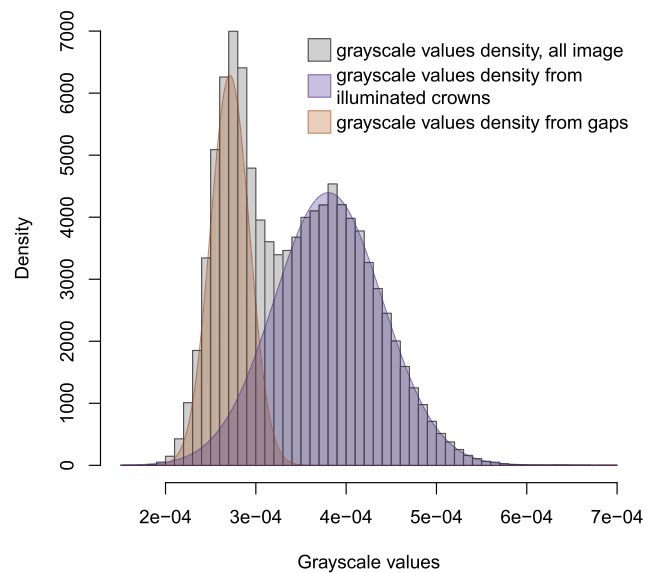

Fig. 2. Distribution of grayscale values of the *Santa Genebra* forest WV-2 image. The bimodal distribution of grayscale values is considered as a mixture distribution of (i) the natural variation in illuminated crowns pixels (blue distribution) and of (ii) the variation of the shaded pixels in the forest gaps and border (red distribution). Both are modeled as normal distributions. (For interpretation of the references to color in this figure legend, the reader is referred to the web version of this article.)

Otherwise, the image resulting from the baseline, Eq. (3), can be retained if the objective is to eliminate small objects with a radius that is smaller than that of the rolling ball:

$$f_i = min(imx_{i-r}, ...,imx_i, ...,imx_{i+r}) \tag{1}$$

$$F_i = max(f_{i-r}, ...,f_i, ...,f_{i+r}) \tag{2}$$

$$b_i = mean(F_{i-r}, ...,F_i, ...,F_{i+r}) \tag{3}$$

$$imx_{corrected,i} = imx_i - b_i \tag{4}$$

Where i is the position of the pixel in the vector of grayscale values of a row of the image *imx* and r is the radius of the rolling ball, Fig. 3. The baseline (b_i, Eq. (3)) is derived as a combination of firstly acquiring the minimum value for each pixel within the rolling ball radius r (f_i, Eq. (1)), from which the maximum value within the defined radius (F_i, Eq. (2)) is determined for each pixel, and then finally this information is incorporated in Eq. (3) (baseline) in which the mean value for each pixel is calculated within the defined radius. Then, the baseline is subtracted from the original image (Eq. (4)). An example of the rolling ball results for a simulated image is provided in Fig. 4. The rolling ball algorithm is implemented in the R package baseline (Liland and Mevik, 2015).

3.1.3. Mathematical morphological operations

Mathematical morphological operators top hat and bottom hat transforms (Serra, 1982) can be used to enhance the contrast of an image based on a structural element (for example a square of n × n pixels). Here, these techniques were used to contrast the shade at the border of the tree crowns and further determine if a pixel was in a tree crown or in the shade between the trees. Considering that $I(x, y)$ is the grayscale image matrix and $M(u, v)$ is the structural element matrix, then erosion and dilation operators are defined as in Eqs. (5) and (6):

$$I \ominus M = min_{u,v}\{I(x + u, y + v) - M(u, v)\} \tag{5}$$

$$I \oplus M = max_{u,v}\{I(x + u, y + v) - M(u, v)\} \tag{6}$$

The opening operator, Eq. (7), is the application of erosion followed by dilation and the closing operator, Eq. (8), is the application of dilation
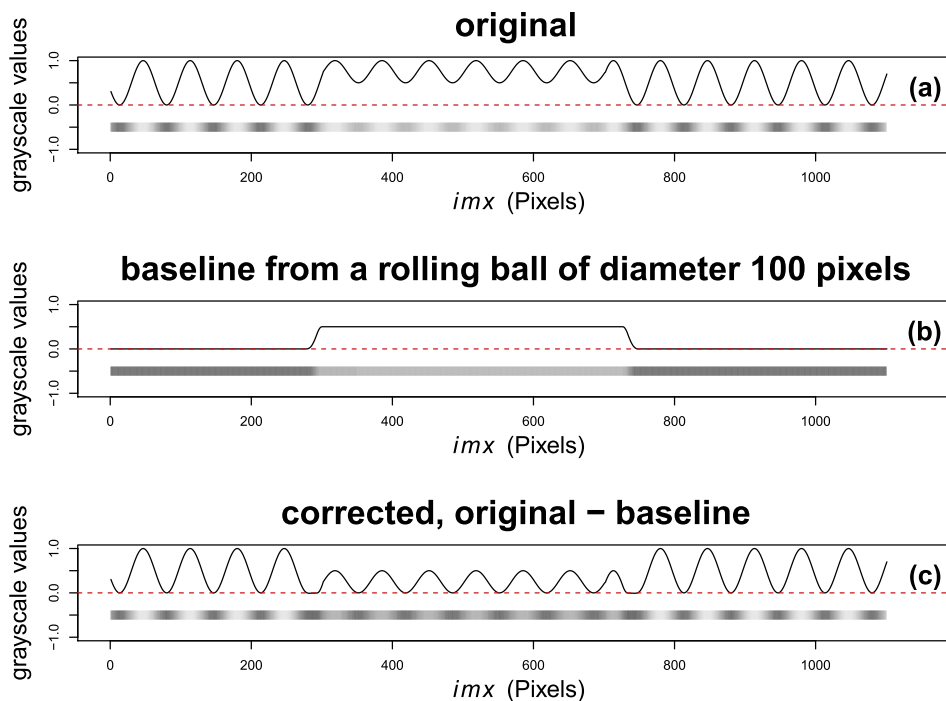
Fig. 3. Rolling ball correction for a row *imx* of a simulated grayscale image. Each graphic presents the signal values in the upper portion and the visual rendering in grayscale values in the lower portion. The original signal is presented in (a). In the baseline (b), only objects with a size larger the ball diameter are preserved. In the corrected image (c), the borders are enhanced and spatial variation of the background intensities with size larger than the ball diameter are eliminated.

followed by erosion:

$$I \circ M = (I \ominus M) \oplus M \qquad (7)$$

$$I \cdot M = (I \oplus M) \ominus M \qquad (8)$$

Then, top hat transform (I_{th}) is defined as the original image minus the image resulting of the opening, Eq. (9) and Fig. 5c, and bottom hat transform (I_{bh}) is defined as the image resulting from the closing minus the original image, Eq. (10) and Fig. 5b:

$$I_{th} = I - (I \circ M) \qquad (9)$$

$$I_{bh} = (I \cdot M) - I \qquad (10)$$

The top and bottom hats can be combined to enhance the contrast of the original image, Eq. (11) and Fig. 5.d.:

$$I_{filtered} = I + I_{th} - I_{bh} \qquad (11)$$

These transformations are implemented in the R package imager (Barthelme, 2017).

3.2. Tree crown delineation algorithm development

The inputs of the tree crown delineation algorithm are the RGB WorldView-2 image pan-sharpened at a 0.5 m spatial resolution with values in 8 bits (0–255) and the shapefile of the forest border. In the following text, we detail the steps of the algorithm.

3.2.1. Image pre-processing

First, the pan-sharpened RGB image was cropped to the forest extent. Then, a 100 m buffer was added to the image and filled with zero values (Fig. 3). This buffer is necessary for the computation of focal statistics and for the segmentation algorithm. Then, a grayscale image was produced by converting the RGB to an HSL image and keeping only the L channel, Fig. 6a. In the *Santa Genebra* reserve, the elevation is relatively smooth and it was not necessary to correct for variation in illumination. In case of large variation in illumination, we suggest to correct the image at this step with a pseudo flat field correction (see Supplementary Fig. S1).

3.2.2. Eliminating area without shade

The *Santa Genebra* reserve contains areas with no or only very few trees and also some dense forest patches around the river with a structure that is different from that of the main forest. In the grayscale image, both areas are characterized by the relative absence of shade. Shaded pixels were identified as the 99th percentile of the distribution of grayscale values in gaps with the EM algorithm (Section 3.1.1). To exclude these areas in the image (areas with few shaded pixels), we count the number of shaded pixels around each pixel in a square of 101 × 101 pixels (50.5 m × 50.5 m). We use this 50.5 m threshold to avoid removing large trees, as some large crowns present very few shaded pixels and because the maximum crown diameter at *Santa Genebra* is ~25 m. Non-shaded areas were identified as pixels below the first percentile of the distribution of the occurrence of shaded pixels in forest (EM algorithm, Section 3.1.1). 887,016 pixels were identified in non-shaded area (~22.175 ha) and were removed from the image by setting these pixels to zero (Fig. 3). This step is unnecessary in cases of homogeneous canopy cover.

3.2.3. First dark object identification

The objective of this step is to begin identifying pixels in the shade of the tree border and set them to zero. The dark pixels were defined as grayscale pixels below the mean of the distribution of grayscale values in gaps (EM-algorithm, Section 3.1.1) and set to zero, Fig. 6b. The mean was used here because some large trees can present holes (shade) in their crown due to tree architecture or crown fragmentation (Rutishauser et al., 2011), and these values have to be retained for further completion.

3.2.4. Filling shade in large tree crowns

This step yields the production of a smoothed image of the maximum grayscale values that will be used to fill the holes in the top of the trees after the next step of identification of large trees. The image was converted to grayscale by first converting the RGB image to HSL and then retaining only the L channel. This grayscale image was inverted, that is, the original grayscale image is multiplied by −1 and the maximum value of the grayscale image is added. This compare to a negative image. We computed two baseline images from a rolling ball filter (see Section 3.1.2) with a radius of 3 pixels following x and y axis,
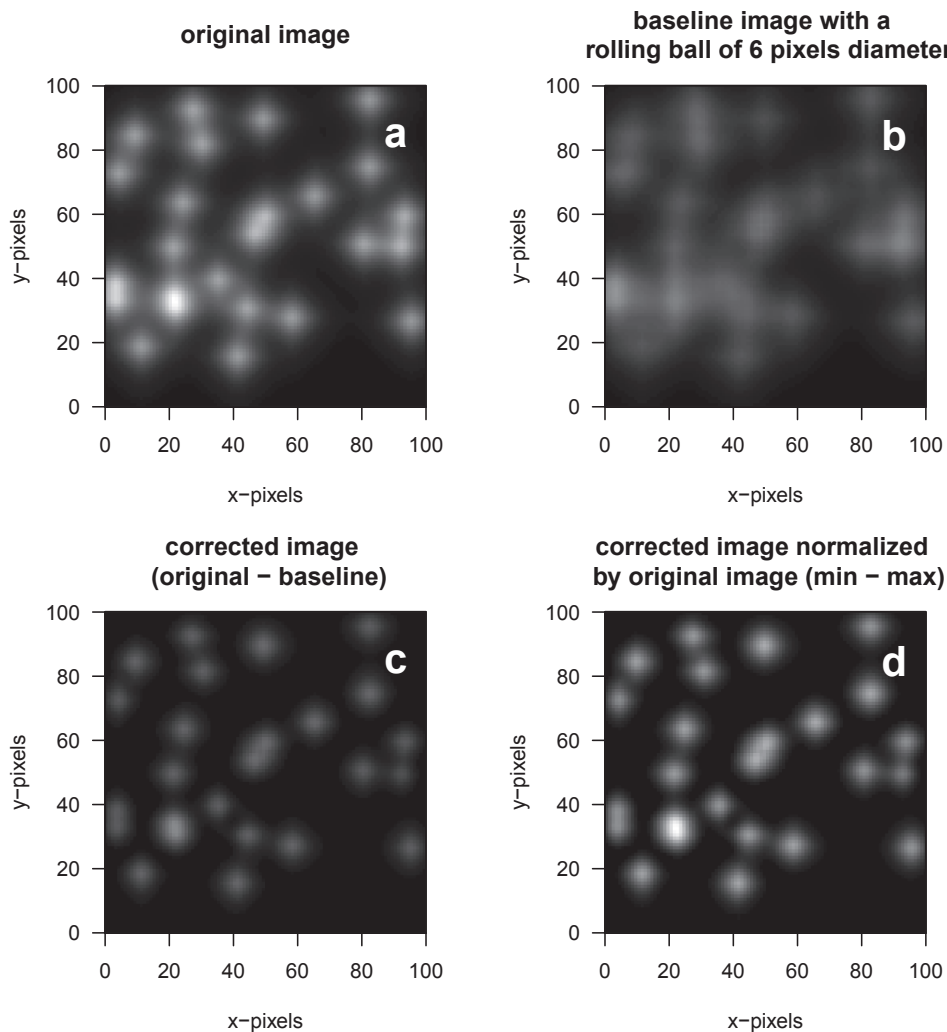
original image

baseline image with a rolling ball of 6 pixels diameter

corrected image (original − baseline)

corrected image normalized by original image (min − max)

Fig. 4. Example of image contrasted with the rolling ball algorithm, with a ball of 6 pixels in diameter. The original image was simulated to present characteristics of the grayscale image of the tree crowns.

then the obtained images were inverted again and the maximum grayscale values of these two last images were used to produce the final image smoothed image, Fig. 6c. This resulting image can be interpreted as the topline image which links all the highest grayscale values with respect to the rolling ball radius.

3.2.5. Identify and filling gaps in large trees

The crowns with a diameter of over 15 pixels (7.5 m) were identified with a top hat transform (see Section 3.1.3) by a circular structuring element with a diameter of 15 pixels, Fig. 6d. The result of the top hat transform is a binary mask containing only the tree crowns that are over 15 pixels in diameter with value 1. The threshold was determined based on the image, that is, not too small because small trees already have homogeneous crown but also not too large because large trees would be underestimated as they present holes (darker area) in the crown, Fig. 6a. The darker areas in the large crowns can be due to tree architecture, large tropical trees can be structured with different crown units (the main branches), or crown fragmentation (Rutishauser et al., 2011). In our image, the threshold of 7.5 m enables the identification of most of the large tree tops, Fig. 6d. The top of the trees were then filled by the grayscale values obtained in the previous step. This step enables the homogenization of the grayscale values in crown structures above 7.5 m in diameter and eliminates most of the shade in the large crowns, which is necessary for the segmentation of the crowns, Fig. 6e.

3.2.6. Second identification of dark objects

After the correction of the shaded pixels in large trees, a final identification of the dark pixels was made, assuming that most of the crown shade has been removed. Here, the dark objects were defined as grayscale pixels below the 99th percentile of the grayscale values distribution in gaps (see Section 3.1.1) and set to zero, Fig. 6f.

3.2.7. Finding small holes in large trees

The large crowns contain isolated pixels of shade that must be filled to further compute the distance of the crown pixel to the edge of the crown (dark pixels outside crowns). These isolated pixels are characterized by the absence or low frequency of pixels with zero values in the neighbouring cells. To find and fill these isolated pixels, we compute the occurrence of non-zero values in a square window of 7×7 pixels around each pixel. The occurrence of non-zero values have a bimodal distribution. The smallest distribution (with smallest mean of non-zero values in the neighborhood) corresponds to the pixels in the crown borders while the highest distribution corresponds to the pixels in the crowns (see Section 3.1.1). Here we define the holes in crowns as pixels with occurrence of non-zero values >75th percentile of occurrence distribution in forest, Fig. 6g. At the end of this step, three classes of pixels are identified: pixels of shade between the trees, non-shaded pixels in the crowns and isolated pixels of shade in the crowns. With these classes, a binary mask was generated, with 0 indicating pixels outside crowns (pixels of shade between the trees) and 1 indicating
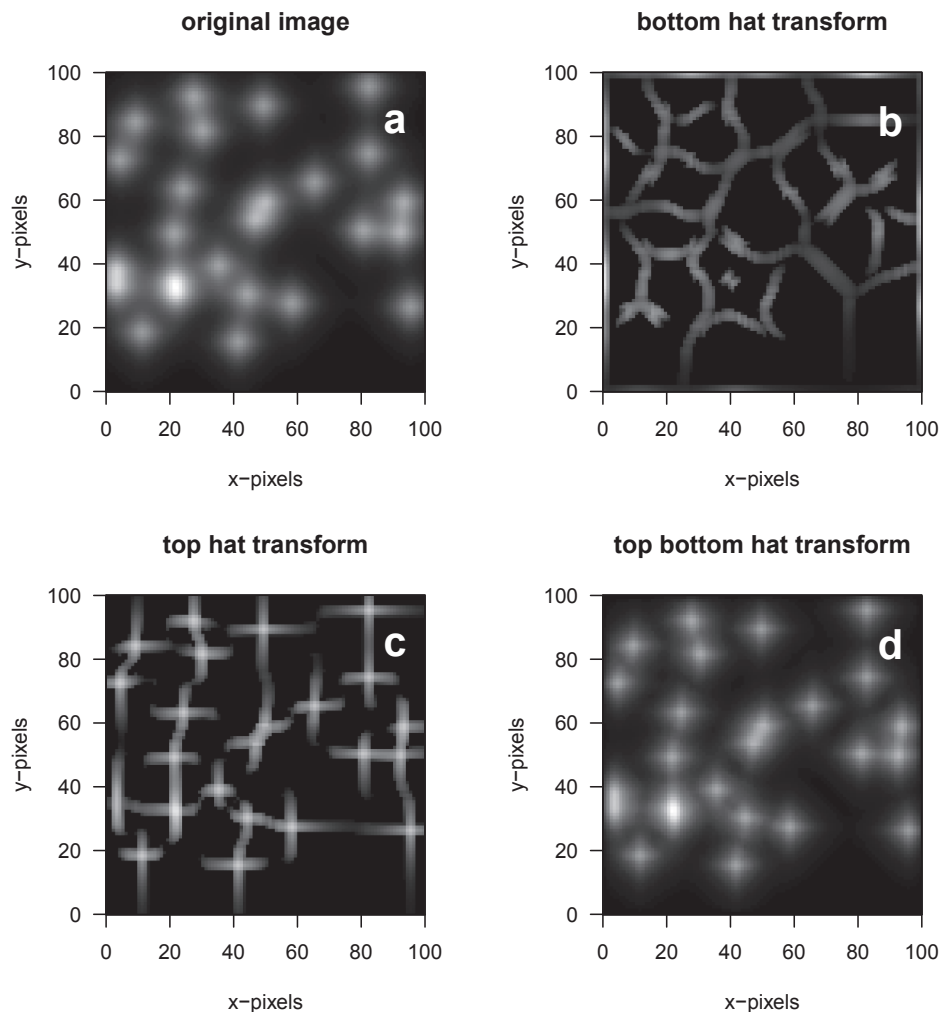
original image

bottom hat transform

top hat transform

top bottom hat transform

Fig. 5. Synthetic example of image contrasted with the top-bottom hat transform with a squared structural of 6 × 6 pixels. The image in (a) was simulated to present characteristics of the grayscale image of tree crowns. To facilitate visualization, the range of values in (b) and (c) are different than of (a) and (d).

pixels inside crowns (non-shaded pixels in the crowns and isolated pixels of shade in the crowns).

3.2.8. Homogenization of grayscale values in large trees

In order to homogenize the grayscale values in the large tree crowns (crowns which concentrated pixels with distance to the border >3.5 m), we first compute the minimum distance between non zero values and zero value with the previous mask. Then, all the pixels with distance >7 pixels of zero values (border) were identified as pixels in large trees. These pixels were filled with the mean of the four highest grayscale values within a square window of 7 × 7 pixels, Fig. 6h.

3.2.9. Extraction of the tree crowns before segmentation

The tree crowns with diameter over 3 m were extracted with a top bottom hat filter with a squared structural element of 6 × 6 pixels (see Section 3.1.3). For the transformed image, we set a threshold at >0.001th percentile (conservative) of the top bottom hat filter to extract tree crowns, Fig. 6i.

3.2.10. Delineation of individual tree crowns

Our segmentation algorithm works with the distance between non-zero and zero value pixels, that is, the distance of the crown pixels to the identified edge. Each identified crown or group of crowns in the pre-segmentation (Fig. 6i) were processed separately. For each crown pixel, the distance to the edge in pixels was computed. Then, local maxima were found within a squared window of the maximum distance

to the edge of the segment. For each local maximum, we created an image by dilating around its location with a square of side twice its value (~ diameter) and attributed 1 to each pixel. Next, we summed the obtained images and removed pixels with zero values. Remaining pixel values equalling one indicate a tree crown, while values greater than one indicate a intersection between the crowns to be removed. Finally, the tree crown polygons were extracted and labeled, Fig. 6j.

This algorithm is computationally demanding and the segmentation part has not been optimized for use in parallel computing systems. *Santa Genebra's* image (3.1 × 2.4 km) was processed with 32 cores (CPUs) and 64-GB RAM in 14 h, 1 h for the pre-segmentation and 13 h for the segmentation. In the pre-segmentation, 30% of the time was consumed by the focal computation. During the segmentation, each segment was processed separately, ~7 min for 100 segments. The algorithm is written in R language (R Core Team, 2016).

3.3. Algorithm validation

To assess the quality of the individual tree delineation, a validation sample of 1001 points was randomly generated over the forest of *Santa Genebra*, Fig. 6k. After removing the random points falling in the areas without shade (see Section 3.2.2), the validation sample was constituted of 989 random points. Then, each point was visually interpreted using the pan-sharpened WorldView-2 images, Fig. 6k. If the point fell in a crown, the value 1 was attributed (true crown) to the point and the crown was manually delineated, else a null value (no
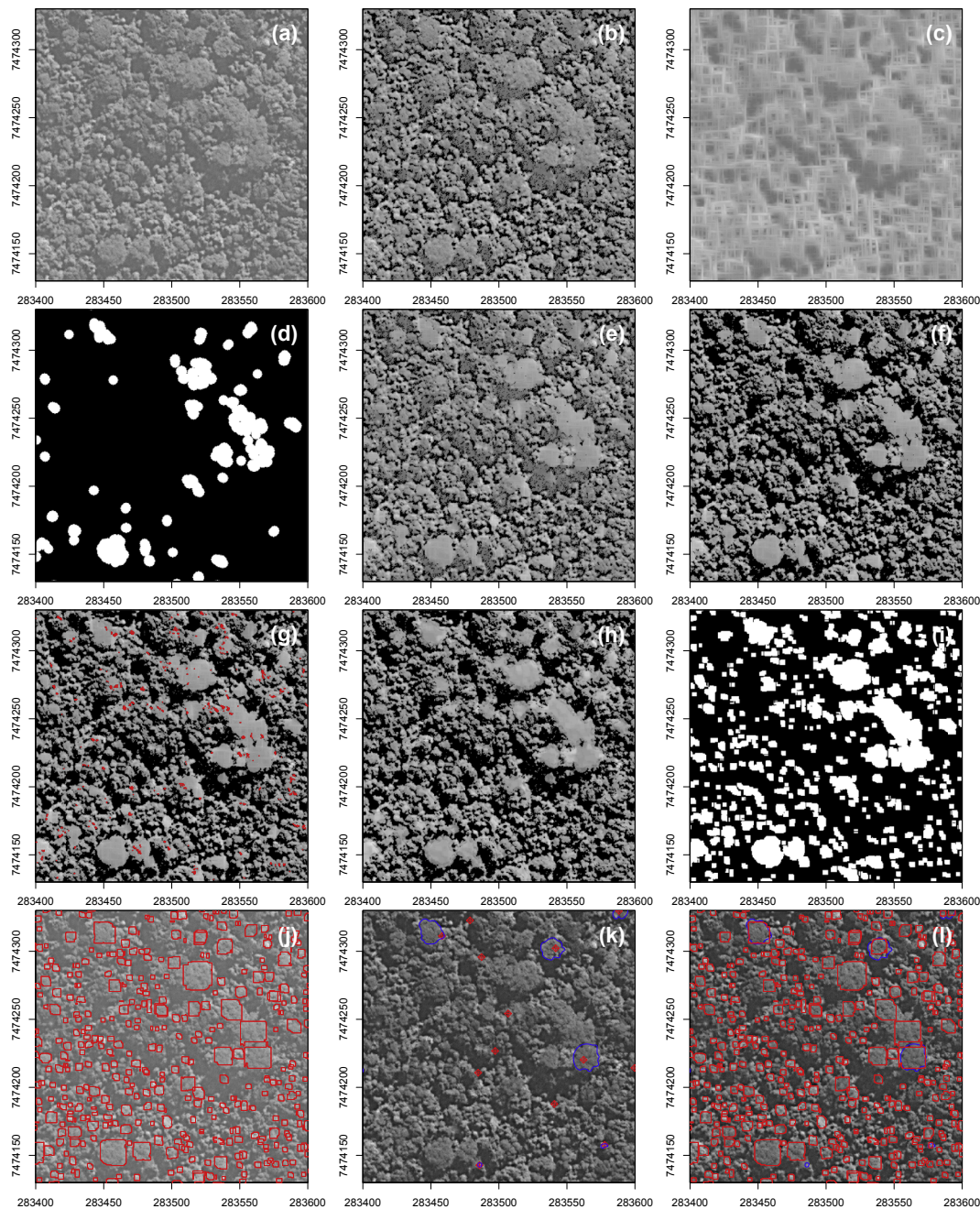
Fig. 6. Details of the algorithm steps for a subset image of the Santa Genebra forest. Grayscale image obtained by converting the RGB bands to an HSL image and retaining only the L channel (a). First dark object identification, grayscale pixels below the mean of the distribution of grayscale values in gaps are set to zero (b). Baseline images from a rolling ball filter with a moving window of 6 pixels to fill the top of the trees after identification of large trees (c). The top of the crowns with a diameter of over 15 pixels identified with a top hat transform (d). Image after removing most of the shaded area in the large crowns with the two previous step (e). Second Dark object identification, grayscale pixels below the 99th percentile of the grayscale values distribution in gaps are set to zero (f). Holes in crowns (in red) identified as pixels with occurrence of non-zero values in the neighbouring cells >75th percentile of occurrence distribution in forest (g). Image after filling the holes in the crowns with the mean of the four highest grayscale values within a square window of 7 × 7 pixels (h). Pre-segmentation, the top of the trees with diameter of over 3 m were extracted with a top bottom hat filter with a squared structural element of 6 × 6 pixels (i). Results of the ITC segmentation (j), where segmented crowns are represented in red. Visual interpretation of the random points (in red) when the point felt in a crown, the crown was manually delineated (in blue) (k). Representation of true (in blue) and segmented crowns (in red) (l). Satellite image courtesy of the . (For interpretation of the references to color in this figure legend, the reader is referred to the web version of this article.)

crown) was attributed to the point (border of tree crowns or gaps). From this visual interpretation, 428 true crowns were found and delineated, and 561 random points were marked as no crown. Then, the confusion matrix between the segmentation results and the random validation sample was generated. The confusion matrix is a table with two rows and two columns that reports the number of true positives (true crowns identified by the algorithm), false positives (crown

identified where there was no crown), false negatives (no crown identified where there were true crowns), and true negatives (no crown identified where there was no crown). From the confusion matrix, the Kappa index and overall accuracy were computed (Cohen, 1968; Foody, 2002). The false negatives were estimated in this step, which are field measured crowns which do not intersect with any crowns from the segmentation, and the false positive, which are the segmented crown

without intersection with visual interpreted crown. Over-segmentation (subdivision of a tree crown into multiple segments) and under-segmentation (segments that contain more than one field measured crown) were described. For each identified crown, pixel excess (number of pixels of the segmented crown outside the true crown) and pixel deficit (number of pixels inside the true crown missing in the segmented crown) were computed. Then, the associations between true crown areas versus pixels deficit or excess were visually assessed by fitting a cubic smooth spline. In addition, the crown size validation was conducted by comparing crown size from the segmented and manual (true) crown delineation with a linear model. Finally, a non-parametric Wilcoxon signed-rank test was used to test for a difference between the crown size distributions of the manually delineated and automatic segmented crowns.

3.4. Spectral validation and tree species mapping

We conducted a spectral validation of the segmentation method by comparing the species classification results between manual and automatic ITC delineation. For classification purposes, we used the eight bands of WorldView-2: Coastal (400–450 nm); Blue (450–510 nm); Green (510–580 nm); Yellow (585–625 nm); Red (630–690 nm); Red Edge (705–745 nm); Near Infrared-1 (770–895 nm) and Near Infrared-2 (860–1040 nm). The image was atmospherically corrected and pan-sharpened using the Fast Line-of-Sight Atmospheric Analysis of Spectral Hypercubes (FLAASH) algorithm (Felde et al., 2003; Solutions, 2009) and the Gram-Schmidt fusion technique (Aiazzi et al., 2009), respectively. In FLAASH, we selected a tropical atmospheric, rural aerosol model and the scene-average visibility was set to 40 km. The Gram-Schmidt spectral sharpening method was selected because it preserves the spectral characteristics of tree species in WorldView-2 images (Cho et al., 2015). The resulting eight pan-sharpened multispectral bands were used for classification.

Pixels from the manually delineated ITCs, Table 1, were extracted from the pan-sharpened WorldView-2 image to compose a dataset with 19 variables, from which eight are spectral band values and 11 are texture features. To obtain texture attributes we first computed basic descriptive statistics of each crown using the panchromatic band (mean, trimmed mean, standard deviation, median, median absolute deviation, minimum, maximum, skew, kurtosis and standard error). Then, we compared the panchromatic band pixel values of each ITC to the respective descriptive statistics. This comparison was conducted in terms of absolute difference. The reasoning of this approach is to explore textural variations arising for species-specific differences in the crown structure. We used the 'psych' R package (Revelle, 2016) to calculate the descriptive statistics. To compare the automatic ITC delineation results with manual ones, we selected only segmented ITCs that presented an overlay area $\geqslant 50\%$ with manual ITCs.

The manual and segmented datasets were randomly partitioned into 70% for training and 30% for testing. During this process, testing and training pixels of the same species were selected from different ITCs, as violations of the ITC identities lead to unrealistic classification accuracies (Baldeck and Asner, 2014). We repeated this procedure 100 times, randomly selecting ITCs to train and test the classifier at each realization and saving the respective reference crowns for accuracy assessment. Systematic changes in the selection of training and testing crowns enable the assessment of the robustness of the classification models and their ability to predict species of unknown samples.

Classification was performed by the support vector machine (SVM) classifier implemented in the 'liquidSVM' R package (Steinwart and Thomann, 2017). SVM is a non-parametric method that separates samples of different classes by constructing hyperplanes in a multi-dimensional space (Vapnik, 1995). Here, we used the Radial Basis Function (RBF-SVM) kernel formulation that has previously showed good results for tree species discrimination in tropical forests (Ferreira et al., 2016; Feret and Asner, 2013; Baldeck and Asner, 2014). RBF-

SVM requires setting the parameters C and γ, which controls, respectively, the trade-off between the complexity and proportion of non-separable samples and the radius of influence of samples selected by the model as support vectors (Cherkassky and Mulier, 2007). The best combination of C and γ for each realization was selected using 5-fold cross validation in the training set. We used a majority-voting rule to assign classes to ITCs, that is, firstly all pixels within a given ITC are classified and thereafter that the most frequent class is assigned to it.

The segmentation method proposed in this work was also tested for the production of a species map. We trained the RBF-SVM classifier using all pixels from the manual delineated ITCs and employed the resulting model to assign classes to the segmented ITCs. This naturally labeled all segments to a given class, leading to a high degree of uncertainty because the forest canopy is composed with hundreds of species. To overcome such a limitation, pixels within segmented ITCs were labeled according to their class probabilities, following Ferreira et al. (2016). Thus, a given pixel x is assigned to a class ω_i if the following condition is satisfied:

$$x \in \omega_i \ if \ p(\omega_i|x) \geqslant \alpha \times max(p(\omega_i)) \tag{12}$$

where $p(\omega_i|x)$ is the probability that ω_i is the correct class for the pixel x, and α is the percentage of the maximum probability value of the class ω_i, $p(\omega_i)$. We set α to 70%, expecting that only pixels with high probabilities that belonged to a given class were labeled.

4. Results

4.1. Detection accuracy

The number of tree crowns correctly detected as a percentage of crowns in the validation dataset was 79.2% (339 out of 428 trees) while 20.8% were not detected (89 false negatives), as shown in Table 2. From the confusion matrix, an overall accuracy of 85.3% and a Kappa index of 0.70 were obtained. 14.2 % of the segmented crowns were detected erroneously (56 false positives). Among the detected trees, 23% were over-segmented (78 crowns, Table 3), that is, more than one segmented crowns intersect with the manually delineated crown (true crown). Among the true crowns, merely 4 (0.9%) were under-segmentated. A representation of true and segmented crowns is presented for a subset image in Fig. 6l.

The mean pixel deficit is of 34.5%, and the mean pixel excess is of 36.8%. While there is no association between pixel deficit and true crown size, as depicted in Fig. 7a, an association exists between pixel excess and true crown size, as depicted in Fig. 7b. Trees with a true crown that is below 100 pixels (5 m^2) have a pixel excess of above 40%.

The association between true and segmented crown size has a coefficient of determination of 0.64, Fig. 7c. The distribution of the difference between the true and segmented crown areas presents a normal shape with a mean of -35.35 pixels and a standard deviation of 188.03 pixels, Fig. 7d.

The crown size distribution of true crowns is significantly different from the segmented crowns, Fig. 8a. After eliminating those tree crowns with less than 100 pixels, no significant difference was found in the distribution of crown size of the segmented and true crown samples, Fig. 8b.

A total of 23,278 crowns were delineated by the algorithm in the

Table 2

Confusion matrix of tree crowns detected by our algorithm intersecting with the manual delineations from the random validation sample (see Section 3.3).

		Segmented crown	
N = 989		NO	YES
True crown	NO	505	56
	YES	89	339

Table 3
Number of segments intersecting with a single true crown and their frequencies. A number of segments of 2 and a frequency of 5 indicates that 2 true crowns detected by our algorithm are intersecting with 5 segmented crowns.

Number of segmented crown intersections with a single true crown	Frequency (%)
1	261 (76.99)
2	55 (16.22)
3	15 (4.42)
4	6 (1.77)
5	2 (0.59)

canopy of the Santa Genebra forest (Supplementary Fig. S2).

4.2. Species classification

The average accuracies for species classification were 65.9% and 62.9% for manual and automatic crown delineation, respectively (Table 4). With the manual crown delineation, two species were classified with an accuracy of above 90%, *Cecropia hololeuca* and *Diatenopteryx sorbifolia*, and two below 60%, *Astronium graveolens* and *Hymenaea courbaril*. With automatic delineation, the accuracy standard deviation was higher except for *Croton piptocalyx*. However, three species were more accurately classified with the automatic delineation, *Cecropia hololeuca* (96.6%), *Cariniana legalis* (62.9%), and *Croton piptocalyx* (80.8%). For *Diatenopteryx sorbifolia*, the automatic delineation accuracy was not reliable, as only 4 crowns were delineated. For

Aspidosperma polyneuron and *Astronium graveolens*, the accuracy using the automatic delineation were both lower than ~10%. For *Hymenaea courbaril*, the classification accuracy was comparable between the two delineation methods – close to 40%.

4.3. Species mapping

Of the 23,278 automatically delineated crowns, 6,355 (27.3%) were identified by the classifier as one of the seven studied species, Fig. 9. For the species with an accuracy of species classification above 80% with automatic tree crown delineation, the classifier identified 1404 *Croton piptocalyx*, 165 *Diatenopteryx sorbifolia* and 152 *Cecropia hololeuca*. For the other species, the classifier identified 514 *Aspidosperma polyneuron*, 1186 *Astronium graveolens*, 2835 *Cariniana legalis* and 99 *Hymenaea courbaril*.

5. Discussion

5.1. Delineation of ITCs

With an estimated accuracy of 80% (Table 2), our method proved useful for crown detection and delineation in tropical forests. As compared to recent studies that employed optical image data to delineate tree crowns, our algorithm yielded results in the range of accuracy reported (68% (Tochon et al., 2015), 88.8% (Dalponte et al., 2014) and 69.2% (Singh et al., 2015)).

Previous studies reported that large and small crown density tends to be underestimated when optical images are used to delineate ITCs
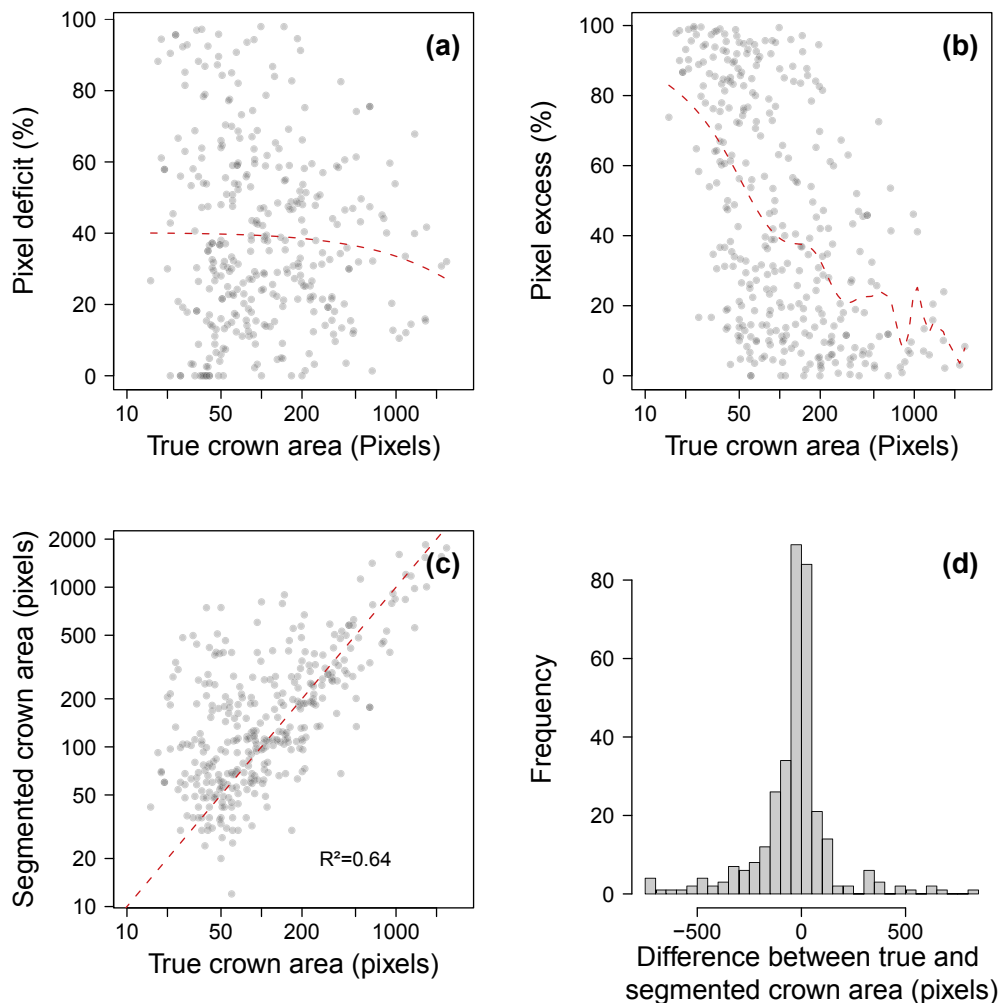

Fig. 7. Association between the true crown area and the pixels deficit per segmented crown (a); between the true crown area and the pixel excess per segmented crown (b); between the true crown area and the segmented crown area (c); and the residuals distribution of the difference between true and segmented crown area (d). The x-axis is in logarithmic scale in (a), (b) and (c). Pixels have an area of 0.25 m². In (a) and (b) the red dashed line is a tendency line fitted by a smooth spline and in (c) the red dashed line is the identity line 1:1. (For interpretation of the references to color in this figure legend, the reader is referred to the web version of this article.)
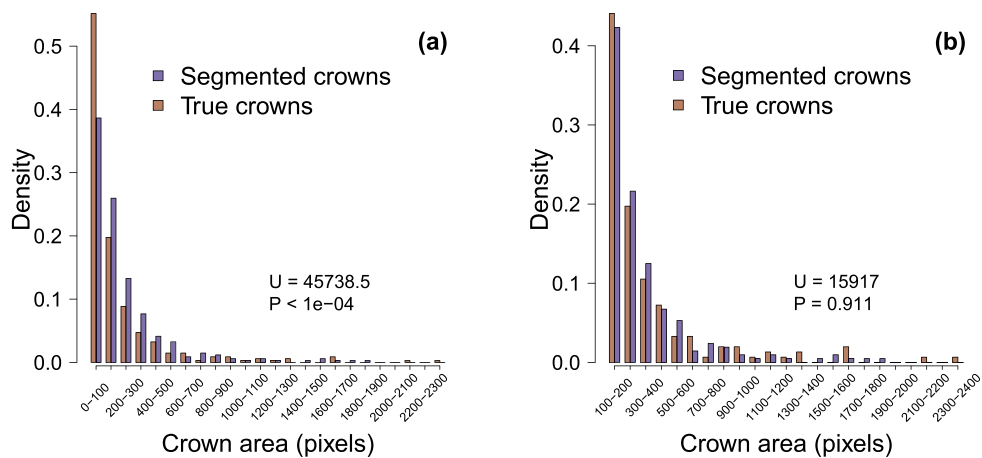
Fig. 8. Segmented and true crown size distribution for all trees (a), and only for trees with a crown area above 100 pixels (b). Statistics of the Wilcoxon signed-rank test are given (U and P values).

Table 4

Accuracy of species classification with manual and automatic tree crown delineation. Crown number indicates the number of crown per species in the manual and in the automatic segmentation. The mean and standard deviation (SD) of classification accuracy were obtained by running SVM classifier 100 times the on the datasets randomly partitioned into 70% for training and 30% for testing (detailed in Section 3.4).

Species	Manual delineation		Automatic delineation	
	Accuracy (mean ± SD, %)	Crowns number	Accuracy (mean ± SD, %)	Crowns number
Aspidosperma polyneuron	60.3 ± 15.8	23	49.8 ± 24.6	17
Astronium graveolens	40.9 ± 10.6	56	30.5 ± 12.6	48
Cariniana legalis	63.8 ± 12.7	50	62.9 ± 15.3	45
Cecropia hololeuca	93.3 ± 6.6	54	96 ± 7.6	29
Croton piptocalyx	68.2 ± 11.6	63	80.8 ± 11.3	51
Diatenopteryx sorbifolia	96.8 ± 5.1	18	80 ± 40.2	4
Hymenaea courbaril	38.2 ± 19.6	18	40.1 ± 25.6	16
Average	65.9 ± 11.7		62.9 ± 19.6	

(Dalponte et al., 2014). Our proposed method does not tend to underestimate the size of large crowns. These crowns show similar pixel deficit and lower pixel excess if compared to the overall samples, Fig. 7a–b, and the segmented crown area shows a good association with the true crown area, Fig. 7c. Emergent trees featuring large crowns such as the species *Cariniana legalis* and *Hymenaea courbaril* tend to have gaps within the crown caused by the shade of thick branches emerging from the main tree stem or dead branches. Such gaps divide the tree crown into two or more parts, thereby increasing the amount of internal-crown shadows and creating boundaries within the crown. Our method is less sensitive to the effects of shade in large tree crowns because it removes shaded pixels and performs a homogenization of the grayscale values within these crowns (Sections 3.2.7 and 3.2.8).

However, our method overestimated the size of small crowns (<5 m^2) and tended to underestimate their density, Figs. 7b and 8a. By removing these trees in the manual and automatic delineation, the actual crown distribution of the study area can be estimated, Fig. 8. Over-segmentation is present in 23% of the delineated crowns. While this is a limitation for tree counting, its impact in species recognition is minimal, as classification accuracy of the species derived from automatic and manual delineated crowns were similar, as depicted in

Table 4.

Another important aspect impacting tree crown delineation in tropical forests using optical images is the effect of shade. It is worth noting that our method is unable to detect understorey trees and trees located in shadowed areas due to other trees or terrain shade, thereby underestimating the total number of trees in the forest stand. Detection of understorey trees and shadowed areas may only be feasible using airborne LiDAR data (Dalponte et al., 2014), but even here the spectral information required to identify the species would remain missing. For a boreal forest, the trees on the ground have been successfully mapped with optical images at a rate of ~42.4% and 28.4% using manual and automatic ITC delineation, respectively (Dalponte et al., 2014). To our knowledge, for tropical forests, the relation between the number of trees on the ground and the number of trees detected in images has not yet been documented. Shade effects arising from terrain elevation might be corrected with a pseudo flat field correction (Supplementary Fig. S1); however in case of steep slopes not exposed to the sun, this method will not work.

Viewing and illumination angles of image acquisition may influence ITC delineation with the proposed method. The effects of the bi-directional reflectance distribution function (BRDF) needs further research because it could affect the shade in the image and our algorithm is based on the detection of shade patterns that create tree crown boundaries. The method is not suitable for open forests, as illuminated pixels from the forest floor will be detected as tree crowns. Moreover, non-forested areas must be removed prior to the image segmentation.

Accounting for local tree phenology is important before selecting the date of the image in order to have the least shade possible in the crown due to leaf fall (de Moura et al., 2017). In seasonal semi-deciduous forests, such as the forest of *Santa Genebra*, the percentage of overstorey trees that present total leaf loss varies from 20% to 50% during the dry season (Ferreira et al., 2016). Our image was taken during the wet season (December), when all the crowns are likely foliated. If a tree crown is not foliated, more shade is present within the crown and the delineation of the tree crown becomes more difficult.

5.2. Algorithm requirements

The proposed algorithm is relatively parsimonious and we make an effort to make it reproducible (code available upon request to the authors). It works with parameters that are mostly based on biological assumptions (distribution of grayscale values in trees and gaps such as observed with LiDAR (Goulamoussène et al., 2017)) and the thresholds can be estimated by using the algorithm or through observations from the image (maximum tree crown for example). However, the initial parameters of the bimodal normal mixture were determined visually
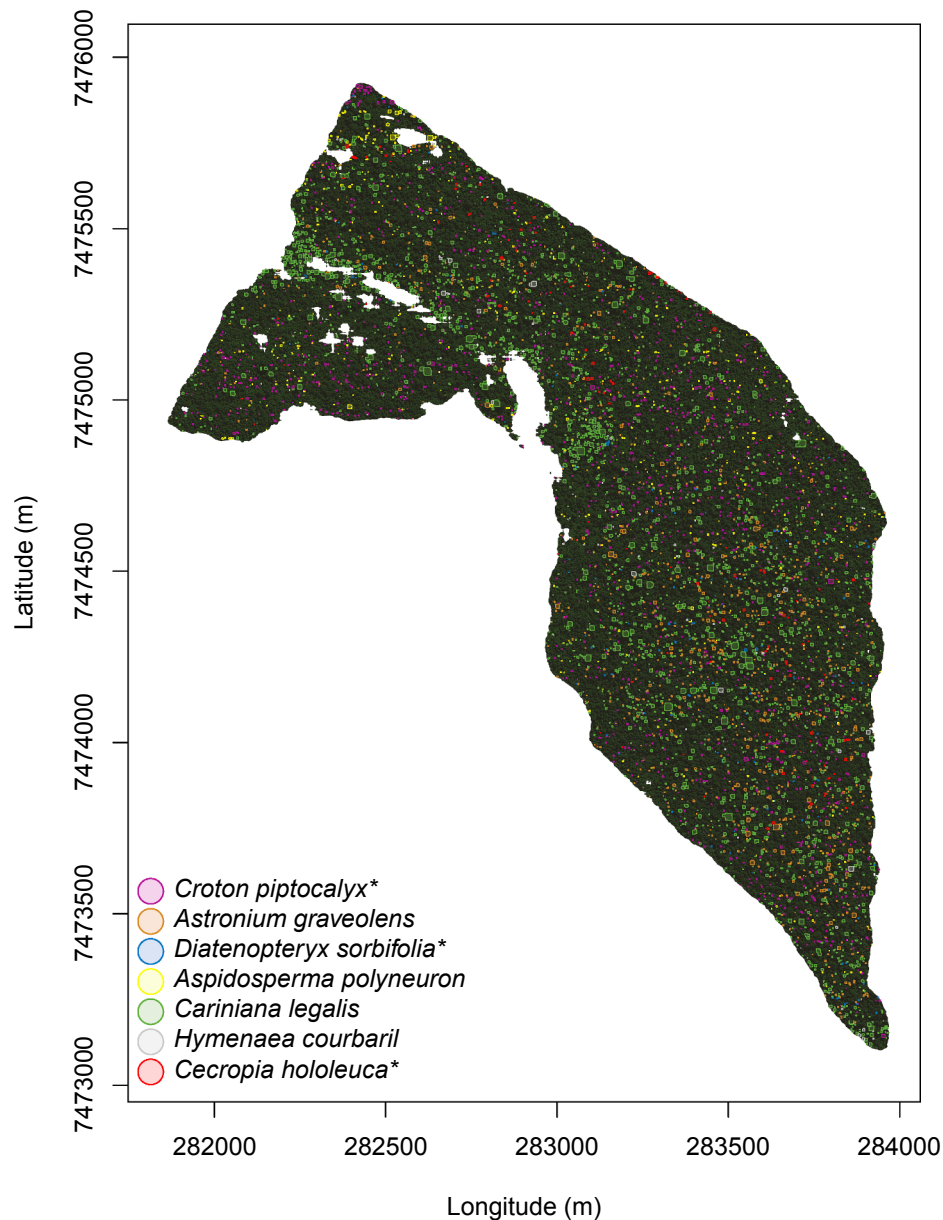
Fig. 9. Map of the seven species derived from the automatic ITC segmentation and produced with Radial Basis Function Support Vector Machines (RBF-SVM) using all the WorldView-2 bands and textural information. * indicates species with an accuracy of species classification of above 80% with automatic tree crown delineation.

with the histogram of grayscale values and set up manually to facilitate EM algorithm convergence.

Our algorithm requires less data than recently developed ITC delineation methods, which need at least aerial VHR image with 0.08 m spatial resolution (Singh et al., 2015), hyperspectral images with 0.4 to 2 m spatial resolution (Tochon et al., 2015; Ferreira et al., 2016; Dalponte et al., 2014) or hyperspectral and LiDAR images with 1.2 m spatial resolution (Lee et al., 2016). Further tests are now needed to determine the accuracy of tree crown delineation with RGB bands from hyperspectral images or using sensors with higher spatial resolution.

The algorithm can be run on forest stands larger than 100 ha on a laptop. However, it is not suitable for small forest stands (<1 ha). Due to the computation of focal statistics, dependent on the size of the moving windows, a border effect could occur. For small forest plots, manual delineation is likely to be more efficient.

5.3. Perspectives for forest biomass and dynamics

In a recent pan-tropical study, the relationship between diameter at breast height and crown area for individual trees has been shown to be very stable, showing no significant inter-site variation (Blanchard et al., 2016), thereby suggesting that diameter and subsequently biomass could be estimated from inverse modeling of the crown size. Another important aspect is that in tropical forests, biomass is concentrated in large trees. For example, in the forest of Paracou (French Guiana), trees with a DBH of above 40 cm comprised 50% of the total above-ground biomass (see Table 1 in Rutishauser et al. (2010)) and similar distributions of the above-ground biomass among the DBH classes have also been observed in the eastern Amazon (Sist et al., 2014). The large trees are likely the ones that are visible in the image and for which our algorithm works well. It is also known that biomass is concentrated in relatively few species (Fauset et al., 2015), which could help to reduce the number of species that must be sampled to derive biomass

estimations from optical images. Furthermore, our delineation could help to track mortality events within a smaller time scale than in the current field inventory (1–5 years census, with a mean time of ~3 years (Mitchard et al., 2014)) and for a significantly larger area. More work is needed to confirm these assumptions and to assess how our algorithm can provide information to estimate biomass and biomass changes in tropical forests. For example, there is potential to use field plot data to help calibrate and validate methods such as ours, and then use WorldView and other imagery to map mortality events at finer temporal resolution and over larger spatial scales.

5.4. Perspectives for tree species mapping

The classification algorithm achieved relatively good accuracies for the seven species, ranging from 38.2% to 96.8% with the manual delineation and 30.5% to 96.0% with the automatic delineation, as indicated in Table 4. This indicates that the spectral information is preserved in the delineated ITCs and that it can be suitable for recognition, at least of some species. In Amazonia 227 (1.4%) of the estimated 16,000 species account for half of all individual trees, while an estimated 11,000 species only account for 0.12% of the total of individuals (ter Steege et al., 2013). Consequently, due to the huge number of species and the rarity of some of them, the botanical determination at the species levels is highly challenging and a large number of species remain undetermined in the field. In Amazonia, some authors measured that less than 70% to 80% of trees can correctly be identified at genus level in field inventories (Guitet et al., 2014; Hawes et al., 2012), and 32% to 67% in Central Africa (Réjou-Méchain et al., 2011). For Amazonia, this rate of identification decreases between 18% and 29% at the species level (Guitet et al., 2014; Hawes et al., 2012). At the species level, these field performances can be compared to the morpho-species classification, commonly employed by botanists with sterile vouchers in the laboratory, whose reliability is evaluated to be between 52% and 67% (Gomes et al., 2013). More work is needed to evaluate how species identification from remote sensing can support species identification operationally in tropical forests. However, it appears that this is likely only feasible for the species with a known accurate determination in the field, and with a high density of individuals per hectare, as a sample of 10 individuals or more are needed to train the algorithm of species recognition. After training on a crown sample with reliable species determination, our method can achieve reasonable species identification, particularly for a large area (above 100 ha). We have to acknowledge that multispectral imagery cannot replace hyperspectral imagery for tropical tree species identification, which records measurement of reflected radiation in hundreds of narrowbands that can detect subtle variations in the chemical and structural attributes of the forest canopy (Ferreira et al., 2016). However, our method is not restricted to multispectral images, and further experiments will be conducted to validate our method with hyperspectral images.

For the species that are well classified, species map like Fig. 9 could help improving species distribution models (SDMs), as one of the prominent limitations of these models are spatial biases in existing occurrence data (He et al., 2015). The species occurrence measurement by satellites is amongst the 10 proposed biodiversity metrics to monitor the progress towards the Aichi Biodiversity Targets (Skidmore et al., 2015); moreover, biodiversity and species assessment to improve knowledge, conservation and management practices is the recommended action to reach the millennium goal 7: "Ensure environmental sustainability" (United Nations, 2005). For conservation, the map of tree species occurrence can also improve estimations of animal resources. For example, leaves and fruits of the genus *Cecropia*, which is identified with an accuracy of above 95% in our species classification (Table 4), are known to be amongst the main food resources of the sloth (Vaughan et al., 2007). If an animal species is associated with a particular tree species, the map of the occurrence of the tree species can help to predict habitat suitability for this species to support the conservation strategy.

5.5. Perspectives for biodiversity mapping

The large areas covered by satellite images could allow the studying of tree spectral diversity patterns and to map canopy diversity at the landscape scale. In pioneering work using hyperspectral image and a pixel based analysis, Feret and Asner (2014) have shown that α- and β-diversity of the canopy could be estimated from an image. With regard to functional diversity, for forests throughout the Andes to the Amazon region in Peru, Asner et al. (2014) have shown that the spectra were dominated by phylogeny within any given community, and spectroscopy accurately classified 85–93% of Amazonian tree species. Functional trait-based approaches offer a promising way to bypass species by not considering the species independently but on a gradient of leaf functional traits, such as leaf nitrogen content, leaf mass area (LMA) or leaf defense compounds including phenols, tannins and lignin (Asner et al., 2014; Asner et al., 2017; Omer et al., 2017). As accurate ITCs delineation reduce the number of pixels outside of the actual crown and improve spectral signatures (Fassnacht et al., 2016) as well as tree species discrimination (Clark et al., 2005; Ferreira et al., 2016; Dalponte et al., 2014), our method could be used to improve the spectral signature of the crown. Further tests must be conducted to describe how the functional and biological biodiversity of species can be estimated with WorldView-2 image.

6. Conclusion

The aims of this work were (i) to develop and evaluate a methodology to efficiently detect and delineate tree crowns in a highly diverse tropical forest using a multispectral image of high-spatial resolution recorded by WorldView-2 and (ii) to test if the spectral signature of the species is conserved in the delineated crown, and if so, produce the forest inventory of seven selected tree species based on field and spectral data and automatic delineated tree crowns.

With regard to the first objective, it was shown that the proposed method of ITC delineation achieved a high detection rate (80.0%), while its main limitations were underestimating small trees and a slight over-segmentation of the crown.

With regard to the second objective, the classification accuracy confirms that the spectra of the species is conserved in the automatic delineated ITC and seven species were classified with reasonable accuracies (30.5–96%) considering that only a pan-sharpened multispectral image was used. Worldview-2 images were shown to be useful for species recognition and could support forest inventory and operational species-mapping at the landscape scale, at least for species such as *Cecropia hololeuca* which the method identifies successfully.

The algorithm will now be tested with remote-sensed images of different spatial and spectral resolutions (Worldview-3 and hyperspectral images). If this validation is conclusive, it will be further used to map species and biochemical leaf properties in tropical forests. First, the automatic delineation will be used to locate trees for field identifications and leaf sampling and, second, to apply the model calibrated with field data (species or leaf characteristics) to all the detected crowns. The consolidation of this methodology could assist large-scale field inventories aiming to better estimate carbon and biodiversity across tropical forests, including the precise mapping of economically, ecologically, and culturally significant resources over large areas.

Appendix A. Supplementary material

Supplementary data associated with this article can be found, in the online version, at https://doi.org/10.1016/j.isprsjprs.2018.09.013.

References

Aiazzi, B., Baronti, S., Lotti, F., Selva, M., 2009. A comparison between global and context-adaptive pansharpening of multispectral images. IEEE Geosci. Remote Sens. Lett. 6, 302–306.

Amaral, C.H., Roberts, D.A., Almeida, T.I., Filho, C.R.S., 2015. Mapping invasive species and spectral mixture relationships with neotropical woody formations in southeastern brazil. {ISPRS} J. Photogramm. Remote Sens. 108, 80–93.

Asner, G.P., Martin, R.E., Carranza-Jimnez, L., Sinca, F., Tupayachi, R., Anderson, C.B., Martinez, P., 2014. Functional and biological diversity of foliar spectra in tree canopies throughout the andes to amazon region. New Phytol. 204, 127–139 2014-1718.

Asner, G.P., Martin, R.E., Knapp, D.E., Tupayachi, R., Anderson, C.B., Sinca, F., Vaughn, N.R., Llactayo, W., 2017. Airborne laser-guided imaging spectroscopy to map forest trait diversity and guide conservation. Science 355, 385–389.

Baccini, A., Goetz, S.J., Walker, W.S., Laporte, N.T., Sun, M., Sulla-Menashe, D., Hackler, J., Beck, P.S.A., Dubayah, R., Friedl, M.A., Samanta, S., Houghton, R.A., 2012. Estimated carbon dioxide emissions from tropical deforestation improved by carbon-density maps. Nat. Clim. Change 2, 182–185.

Baldeck, C.A., Asner, G.P., 2014. Improving remote species identification through efficient training data collection. Remote Sens. 6, 2682–2698.

Barthelme, S., 2017. imager: Image Processing Library Based on 'CImg'. R package version 0.40.1.

Benaglia, T., Chauveau, D., Hunter, D.R., Young, D., 2009. mixtools: an R package for analyzing finite mixture models. J. Stat. Softw. 32, 1–29.

Blanchard, E., Birnbaum, P., Ibanez, T., Boutreux, T., Antin, C., Ploton, P., Vincent, G., Pouteau, R., Vandrot, H., Hequet, V., Barbier, N., Droissart, V., Sonké, B., Texier, N., Kamdem, N.G., Zebaze, D., Libalah, M., Couteron, P., 2016. Contrasted allometries between stem diameter, crown area, and tree height in five tropical biogeographic areas. Trees 30, 1953–1968.

Brienen, R.J.W., Phillips, O.L., Feldpausch, T.R., Gloor, E., Baker, T.R., Lloyd, J., Lopez-Gonzalez, G., Monteagudo-Mendoza, A., Malhi, Y., Lewis, S.L., Vasquez Martinez, R., Alexiades, M., Alvarez Davila, E., Alvarez-Loayza, P., Andrade, A., Aragao, L.E.O.C., Araujo-Murakami, A., Arets, E.J.M.M., Arroyo, L., Aymard, G.A., Banki, O.S., Baraloto, C., Barroso, J., Bonal, D., Boot, R.G.A., Camargo, J.L.C., Castilho, C.V., Chama, V., Chao, K.J., Chave, J., Comiskey, J.A., Cornejo Valverde, F., da Costa, L., de Oliveira, E.A., Di Fiore, A., Erwin, T.L., Fauset, S., Forsthofer, M., Galbraith, D.R., Grahame, E.S., Groot, N., Herault, B., Higuchi, N., Honorio Coronado, E.N., Keeling, H., Killeen, T.J., Laurance, W.F., Laurance, S., Licona, J., Magnussen, W.E., Marimon, B.S., Marimon-Junior, B.H., Mendoza, C., Neill, D.A., Nogueira, E.M., Nunez, P., Pallqui Camacho, N.C., Parada, A., Pardo-Molina, G., Peacock, J., Pena-Claros, M., Pickavance, G.C., Pitman, N.C.A., Poorter, L., Prieto, A., Quesada, C.A., Ramirez, F., Ramirez-Angulo, H., Restrepo, Z., Roopsind, A., Rudas, A., Salomao, R.P., Schwarz, M., Silva, N., Silva-Espejo, J.E., Silveira, M., Stropp, J., Talbot, J., ter Steege, H., Teran-Aguilar, J., Terborgh, J., Thomas-Caesar, R., Toledo, M., Torello-Raventos, M., Umetsu, R.K., van der Heijden, G.M.F., van der Hout, P., Guimaraes Vieira, I.C., Vieira, S.A., Vilanova, E., Vos, V.A., Zagt, R.J., 2015. Long-term decline of the amazon carbon sink. Nature 519, 344–348.

Bunting, P., He, W., Zwiggelaar, R., Lucas, R., 2009. Combining Texture and Hyperspectral Information for the Classification of Tree Species in Australian Savanna Woodlands. Springer Berlin Heidelberg, Berlin, Heidelberg, pp. 19–26.

Caughlin, T.T., Graves, S.J., Asner, G.P., van Breugel, M., Hall, J.S., Martin, R.E., Ashton, M.S., Bohlman, S.A., 2016. A hyperspectral image can predict tropical tree growth rates in single-species stands. Ecol. Appl. 26, 2369–2375.

Cherkassky, V., Mulier, F.M., 2007. Learning from Data: Concepts, Theory, and Methods, second ed. John Wiley & Sons, Hoboken.

Cho, M.A., Mathieu, R., Asner, G.P., Naidoo, L., van Aardt, J., Ramoelo, A., Debba, P., Wessels, K., Main, R., Smit, I.P., Erasmus, B., 2012. Mapping tree species composition in south african savannas using an integrated airborne spectral and lidar system. Remote Sens. Environ. 125, 214–226.

Cho, M.A., Malahlela, O., Ramoelo, A., 2015. Assessing the utility worldview-2 imagery for tree species mapping in south african subtropical humid forest and the conservation implications: Dukuduku forest patch as case study. Int. J. Appl. Earth Obser. Geoinform. 38, 349–357.

Clark, M.L., Roberts, D.A., Clark, D.B., 2005. Hyperspectral discrimination of tropical rain forest tree species at leaf to crown scales. Remote Sens. Environ. 96, 375–398.

Cohen, J., 1968. Weighted kappa: nominal scale agreement provision for scaled disagreement or partial credit. Psychol. Bull. 70, 213.

Condit, R., Ashton, P.S., Manokaran, N., LaFrankie, J.V., Hubbell, S.P., Foster, R.B., 1999. Dynamics of the forest communities at pasoh and barro colorado: comparing two 50–ha plots. Philosoph. Trans. Roy. Soc. Lond. B: Biol. Sci. 354, 1739–1748.

CRU TS3.21, 2014. The Climate Data Guide: CRU TS3.21 Gridded precipitation and other meteorological variables since 1901. Technical report. National Center for Atmospheric Research Staff (Eds). Retrieved from < https://climatedataguide.ucar.edu/climate-data/cru-ts321-gridded-precipitation-and-other-meteorological-variables-1901 > (last modified 20 Aug 2014).

Culvenor, D.S., 2002. Tida: an algorithm for the delineation of tree crowns in high spatial resolution remotely sensed imagery. Comput. Geosci. 28, 33–44.

Dalponte, M., Orka, H.O., Ene, L.T., Gobakken, T., Naesset, E., 2014. Tree crown delineation and tree species classification in boreal forests using hyperspectral and ALS data. Remote Sens. Environ. 140, 306–317.

de Lima, R.A.F., Mori, D.P., Pitta, G., Melito, M.O., Bello, C., Magnago, L.F., Zwiener, V.P., Saraiva, D.D., Marques, M.C.M., de Oliveira, A.A., Prado, P.I., 2015. How much do we know about the endangered atlantic forest? Reviewing nearly 70 years of information on tree community surveys. Biodivers. Conserv. 24, 2135–2148.

de Moura, Y.M., Galvo, L.S., Hilker, T., Wu, J., Saleska, S., do Amaral, C.H., Nelson, B.W., Lopes, A.P., Wiedeman, K.K., Prohaska, N., de Oliveira, R.C., Machado, C.B., Arago, L.E., 2017. Spectral analysis of amazon canopy phenology during the dry season using a tower hyperspectral camera and modis observations. ISPRS J. Photogramm. Remote Sens. 131, 52–64.

DigitalGlobe, 2017. DigitalGlobe Core Imagery Product Guide.

Duncanson, L., Cook, B., Hurtt, G., Dubayah, R., 2014. An efficient, multi-layered crown delineation algorithm for mapping individual tree structure across multiple ecosystems. Remote Sens. Environ. 154, 378–386.

Erickson, M., 2004. Segmentation and Classification of Individual Tree Crowns in High Spatial Resolution Aerial Images (Ph.D. thesis). Swedish University of Agricultural Sciences, Uppsala.

FAO (Ed.), 2016. State of the Worlds Forests 2016. Forests and Agriculture: Land-use Challenges and Opportunities. Food and Agriculture Organization of the United Nations, Rome.

Farah, F.T., Rodrigues, R.R., Santos, F.A.M., Tamashiro, J.Y., Shepherd, G.J., Siqueira, T., Batista, J.L.F., Manly, B.J.F., 2014. Forest destructuring as revealed by the temporal dynamics of fundamental species. Case study of Santa Genebra Forest in Brazil. Ecol. Indicat. 37, 40–44.

Fassnacht, F.E., Latifi, H., Stereczak, K., Modzelewska, A., Lefsky, M., Waser, L.T., Straub, C., Ghosh, A., 2016. Review of studies on tree species classification from remotely sensed data. Remote Sens. Environ. 186, 64–87.

Fauset, S., Johnson, M.O., Gloor, M., Baker, T.R., M, A.M., Brienen, R.J.W., Feldpausch, T.R., Lopez-gonzalez, G., Terborgh, J.W., Ruokolainen, K., Silveira, M., Laurance, S.G.W., Laurance, W.F., Costa, R.C., Levis, C., Schietti, J., Souza, P., Arets, E., Moscoso, V.C., Castro, W., Coronado, E.N.H., Pen, M., Quesada, C.A., Stropp, J., Vieira, S.A., Steininger, M., Rodr, C.R., 2015. Hyperdominance in Amazonian forest carbon cycling. Nat. Commun. 1–9.

Felde, G.W., Anderson, G.P., Cooley, T.W., Matthew, M.W., adler Golden, S.M., Berk, A., Lee, J., 2003. Analysis of hyperion data with the flaash atmospheric correction algorithm. In: IGARSS 2003. 2003 IEEE International Geoscience and Remote Sensing Symposium. Proceedings (IEEE Cat. No.03CH37477), vol. 1, pp. 90–92.

Feret, J.B., Asner, G.P., 2013. Tree species discrimination in tropical forests using airborne imaging spectroscopy. IEEE Trans. Geosci. Remote Sens. 51, 73–84.

Feret, J.-B., Asner, G.P., 2014. Mapping tropical forest canopy diversity using high-fidelity imaging spectroscopy. Ecol. Appl. 24, 1289–1296.

Ferreira, M.P., Zortea, M., Zanotta, D.C., Shimabukuro, Y.E., de Souza Filho, C.R., 2016. Mapping tree species in tropical seasonal semi-deciduous forests with hyperspectral and multispectral data. Remote Sens. Environ. 179, 66–78.

Foody, G.M., 2002. Status of land cover classification accuracy assessment. Remote Sens. Environ. 80, 185–201.

Gangkofner, U.G., Pradhan, P.S., Holcomb, D.W., 2008. Optimizing the high-pass filter addition technique for image fusion. Photogramm. Eng. Remote Sens. 74, 1107–1118.

Gomes, A.C., Andrade, A., Barreto-Silva, J.S., Brenes-Arguedas, T., Lpez, D.C., de Freitas, C.C., Lang, C., de Oliveira, A.A., Prez, A.J., Perez, R., da Silva, J.B., Silveira, A.M., Vaz, M.C., Vendrami, J., Vicentini, A., 2013. Local plant species delimitation in a highly diverse amazonian forest: do we all see the same species? J. Veget. Sci. 24, 70–79.

Goulamoussène, Y., Bedeau, C., Descroix, L., Linguet, L., Hérault, B., 2017. Environmental control of natural gap size distribution in tropical forests. Biogeosciences 14, 353–364.

GRASS Development Team, 2017. Geographic Resources Analysis Support System (GRASS GIS) Software, Version 7.2. Open Source Geospatial Foundation.

Guaratini, M.T.G., Gomes, E.C.P., Tamashiro, J.Y., Rodrigues, R.R., 2008. Composio florstica da reserva municipal de santa genebra, campinas, sp. Revista Brasileira de Botanica 31, 323–337.

Guitet, S., Sabatier, D., Brunaux, O., Hrault, B., Aubry-Kientz, M., Molino, J.-F., Baraloto, C., 2014. Estimating tropical tree diversity indices from forestry surveys: a method to integrate taxonomic uncertainty. For. Ecol. Manage. 328, 270–281.

Hawes, J.E., Peres, C.A., Riley, L.B., Hess, L.L., 2012. Landscape-scale variation in structure and biomass of amazonian seasonally flooded and unflooded forests. For. Ecol. Manage. 281, 163–176.

Heenkenda, M.K., Joyce, K.E., Maier, S.W., Bartolo, R., 2014. Mangrove species identification: comparing worldview-2 with aerial photographs. Remote Sens. 6, 6064–6088.

He, K.S., Bradley, B.A., Cord, A.F., Rocchini, D., Tuanmu, M.-N., Schmidtlein, S., Turner, W., Wegmann, M., Pettorelli, N., 2015. Will remote sensing shape the next generation of species distribution models? Remote Sens. Ecol. Conserv. 1, 4–18.

Immitzer, M., Atzberger, C., Koukal, T., 2012. Tree species classification with random forest using very high spatial resolution 8-band worldview-2 satellite data. Remote Sens. 4, 2661–2693.

Kalacska, M., Bohlman, S., Sanchez-Azofeifa, G., Castro-Esau, K., Caelli, T., 2007.

Hyperspectral discrimination of tropical dry forest lianas and trees: comparative data reduction approaches at the leaf and canopy levels. Remote Sens. Environ. 109, 406–415.

Ke, Y., Quackenbush, L.J., 2011. A review of methods for automatic individual tree-crown detection and delineation from passive remote sensing. Int. J. Remote Sens. 32, 4725–4747.

Kneen, M.A., Annegarn, H.J., 1996. Algorithm for fitting XRF, SEM and PIXE X-ray spectra backgrounds. Nucl. Instrum. Methods Phys. Res., Sect. B: Beam Interact. Mater. Atoms 109–110, 209–213.

Latif, Z.A., Zamri, I., Omar, H., 2012. Determination of tree species using worldview-2 data. In: 2012 IEEE 8th International Colloquium on Signal Processing and its Applications, pp. 383–387.

Laurin, G.V., Chen, Q., Lindsell, J.A., Coomes, D.A., Frate, F.D., Guerriero, L., Pirotti, F., Valentini, R., 2014. Above ground biomass estimation in an african tropical forest with lidar and hyperspectral data. {ISPRS} J. Photogramm. Remote Sens. 89, 49–58.

Leckie, D.G., Gougeon, F.A., Walsworth, N., Paradine, D., 2003. Stand delineation and composition estimation using semi-automated individual tree crown analysis. Remote Sens. Environ. 85, 355–369.

Lee, J., Cai, X., Lellmann, J., Dalponte, M., Malhi, Y., Butt, N., Morecroft, M., Sch, C.-b., Coomes, D.A., 2016. Individual tree species classification from airborne multisensor imagery using robust PCA. IEEE J. Sel. Top. Appl. Earth Obser. Remote Sens. 9, 2554–2567.

Leito Filho, H., Morellato, P., 1995. A vegetao da Reserva de Santa Genebra. Ecologia e preservao de uma floresta tropical urbana. Editora da UNICAMP, Campinas, Brazil.

Liland, K.H., Mevik, B.-H., 2015. baseline: Baseline Correction of Spectra, 2015. R package version 1.2-1.

Lopes, A., Nelson, B., Wu, J., Graa, P., Tavares, J., Prohaska, N., Martins, G., Saleska, S., 2016. Leaf flush drives dry season green-up of the central amazon. Remote Sens. Environ. 182, 90–98.

Mitchard, E.T.A., Feldpausch, T.R., Brienen, R.J.W., Lopez-Gonzalez, G., Monteagudo, A., Baker, T.R., Lewis, S.L., Lloyd, J., Quesada, C.A., Gloor, M., ter Steege, H., Meir, P., Alvarez, E., Araujo-Murakami, A., Arago, L.E.O.C., Arroyo, L., Aymard, G., Banki, O., Bonal, D., Brown, S., Brown, F.I., Cern, C.E., Chama Moscoso, V., Chave, J., Comiskey, J.A., Cornejo, F., Corrales Medina, M., Da Costa, L., Costa, F.R.C., Di Fiore, A., Domingues, T.F., Erwin, T.L., Frederickson, T., Higuchi, N., Honorio Coronado, E.N., Killeen, T.J., Laurance, W.F., Levis, C., Magnusson, W.E., Marimon, B.S., Marimon Junior, B.H., Mendoza Polo, I., Mishra, P., Nascimento, M.T., Neill, D., Nez Vargas, M.P., Palacios, W.A., Parada, A., Pardo Molina, G., Pea-Claros, M., Pitman, N., Peres, C.A., Poorter, L., Prieto, A., Ramirez-Angulo, H., Restrepo Correa, Z., Roopsind, A., Roucoux, K.H., Rudas, A., Salomo, R.P., Schietti, J., Silveira, M., de Souza, P.F., Steininger, M.K., Stropp, J., Terborgh, J., Thomas, R., Toledo, M., Torres-Lezama, A., van Andel, T.R., van der Heijden, G.M.F., Vieira, I.C.G., Vieira, S., Vilanova-Torre, E., Vos, V.A., Wang, O., Zartman, C.E., Malhi, Y., Phillips, O.L., 2014. Markedly divergent estimates of amazon forest carbon density from ground plots and satellites. Global Ecol. Biogeogr. 23, 935–946.

Mutanga, O., Adam, E., Cho, M.A., 2012. High density biomass estimation for wetland vegetation using worldview-2 imagery and random forest regression algorithm. Int. J. Appl. Earth Obser. Geoinform. 18, 399–406.

Nikolakopoulos, K., Oikonomidis, D., 2015. Quality assessment of ten fusion techniques applied on worldview-2. Eur. J. Remote Sens. 48, 141–167.

Oliveira-Filho, A.T., Ratterf, J.A.a., 1995. A study of the origin of central brazilian forests by the analysis of plant species distribution patterns. Edinb. J. Bot. 52, 141–194.

Omer, G., Mutanga, O., Abdel-Rahman, E.M., Peerbhay, K., Adam, E., 2017. Mapping leaf nitrogen and carbon concentrations of intact and fragmented indigenous forest ecosystems using empirical modeling techniques and worldview-2 data. {ISPRS} J. Photogramm. Remote. 131, 26–39.

Palace, M., Keller, M., Asner, G.P., Hagen, S., Braswell, B., 2008. Amazon forest structure from ikonos satellite data and the automated characterization of forest canopy properties. Biotropica 40, 141–150.

Pan, Y., Birdsey, R.A., Fang, J., Houghton, R., Kauppi, P.E., Kurz, W.A., Phillips, O.L., Shvidenko, A., Lewis, S.L., Canadell, J.G., Ciais, P., Jackson, R.B., Pacala, S.W., McGuire, A.D., Piao, S., Rautiainen, A., Sitch, S., Hayes, D., 2011. A large and persistent carbon sink in the world's forests. Science 333, 988–993.

Peerbhay, K.Y., Mutanga, O., Ismail, R., 2014. Investigating the capability of few strategically placed worldview-2 multispectral bands to discriminate forest species in Kwazulu-Natal, South Africa. IEEE J. Sel. Top. Appl. Earth Obser. Remote Sens. 7, 307–316.

Phillips, O.L., Brienen, R.J.W., 2017. Carbon uptake by mature amazon forests has mitigated amazon nations' carbon emissions. Carbon Balance Manage. 12, 1.

Phillips, O.L., Aragao, L.E.O.C., Lewis, S.L., Fisher, J.B., Lloyd, J., Lopez-Gonzalez, G., Malhi, Y., Monteagudo, A., Peacock, J., Quesada, C.A., van der Heijden, G., Almeida, S., Amaral, I., Arroyo, L., Aymard, G., Baker, T.R., Banki, O., Blanc, L., Bonal, D., Brando, P., Chave, J., Alves de Oliveira, A.C., Cardozo, N.D., Czimczik, C.I., Feldpausch, T.R., Freitas, M.A., Gloor, E., Higuchi, N., Jimenez, E., Lloyd, G., Meir, P., Mendoza, C., Morel, A., Neill, D.A., Nepstad, D., Patino, S., Cristina Penuela, M., Prieto, A., Ramirez, F., Schwarz, M., Silva, J., Silveira, M., Thomas, A.S., ter Steege, H., Stropp, J., Vasquez, R., Zelazowski, P., Alvarez Davila, E., Andelman, S., Andrade, A., Chao, K.-J., Erwin, T., Di Fiore, A., Honorio C, E., Keeling, H., Killeen, T.J., Laurance, W.F., Pena Cruz, A., Pitman, N.C.A., Nunez Vargas, P., Ramirez-Angulo, H., Rudas, A., Salamao, R., Silva, N., Terborgh, J., Torres-Lezama, A., 2009. Drought sensitivity of the Amazon rainforest. Science 323, 1344–1347.

Pu, R., Landry, S., 2012. A comparative analysis of high spatial resolution ikonos and worldview-2 imagery for mapping urban tree species. Remote Sens. Environ. 124, 516–533.

Pu, R., Landry, S., Zhang, J., 2015. Evaluation of atmospheric correction methods in identifying urban tree species with worldview-2 imagery. IEEE J. Sel. Top. Appl.

Earth Obser. Remote Sens. 8, 1886–1897.

R Core Team, 2016. R: A Language and Environment for Statistical Computing. R Foundation for Statistical Computing, Vienna, Austria.

Revelle, W., 2016. psych: Procedures for Psychological, Psychometric, and Personality Research. Northwestern University, Evanston, Illinois R package version 1.6.9.

Réjou-Méchain, M., Fayolle, A., Nasi, R., Gourlet-Fleury, S., Doucet, J.-L., Gally, M., Hubert, D., Pasquier, A., Billand, A., 2011. Detecting large-scale diversity patterns in tropical trees: Can we trust commercial forest inventories? For. Ecol. Manage. 261, 187–194.

Rutishauser, E., Wagner, F., Herault, B., Nicolini, E.-A., Blanc, L., 2010. Contrasting above-ground biomass balance in a neotropical rain forest. J. Veget. Sci. 21, 672–682.

Rutishauser, E., Barthlmy, D., Blanc, L., Eric-Andr, N., 2011. Crown fragmentation assessment in tropical trees: method, insights and perspectives. For. Ecol. Manage. 261, 400–407.

Saatchi, S., Mascaro, J., Xu, L., Keller, M., Yang, Y., Duffy, P., Esprito-Santo, F., Baccini, A., Chambers, J., Schimel, D., 2015. Seeing the forest beyond the trees. Global Ecol. Biogeogr. 24, 606–610.

Serra, J., 1982. Image Analysis and Mathematical Morphology, volume I of ISBN 0-12-637240-3. Academic Press.

Singh, M., Evans, D., Tan, B.S., Nin, C.S., 2015. Mapping and characterizing selected canopy tree species at the Angkor world heritage site in cambodia using aerial data. PLOS ONE 10, 1–26.

Sist, P., Mazzei, L., Blanc, L., Rutishauser, E., 2014. Large trees as key elements of carbon storage and dynamics after selective logging in the eastern amazon. For. Ecol. Manage. 318, 103–109.

Skidmore, A.K., Pettorelli, N., Coops, N.C., Geller, G.N., Hansen, M., Lucas, R., Mcher, C.A., O'Connor, B., Paganini, M., Pereira, H.M., Schaepman, M.E., Turner, W., Wang, T., Wegmann, M., 2015. Environmental science: agree on biodiversity metrics to track from space. Nat. News.

Slik, J.W.F., Arroyo-Rodrguez, V., Aiba, S.-I., Alvarez-Loayza, P., Alves, L.F., Ashton, P., Balvanera, P., Bastian, M.L., Bellingham, P.J., van den Berg, E., Bernacci, L., da Conceio Bispo, P., Blanc, L., Bhning-Gaese, K., Boeckx, P., Bongers, F., Boyle, B., Bradford, M., Brearley, F.Q., Breuer-Ndoundou Hockemba, M., Bunyavejchewin, S., Calderado Leal Matos, D., Castillo-Santiago, M., Catharino, E.L.M., Chai, S.-L., Chen, Y., Colwell, R.K., Chazdon, R.L., Clark, C., Clark, D.B., Clark, D.A., Culmsee, H., Damas, K., Dattaraja, H.S., Dauby, G., Davidar, P., DeWalt, S.J., Doucet, J.-L., Duque, A., Durigan, G., Eichhorn, K.A.O., Eisenlohr, P.V., Eler, E., Ewango, C., Farwig, N., Feeley, K.J., Ferreira, L., Field, R., de Oliveira Filho, A.T., Fletcher, C., Forshed, O., Franco, G., Fredriksson, G., Gillespie, T., Gillet, J.-F., Amarnath, G., Griffith, D.M., Grogan, J., Gunatilleke, N., Harris, D., Harrison, R., Hector, A., Homeier, J., Imai, N., Itoh, A., Jansen, P.A., Joly, C.A., de Jong, B.H.J., Kartawinata, K., Kearsley, E., Kelly, D.L., Kenfack, D., Kessler, M., Kitayama, K., Kooyman, R., Larney, E., Laumonier, Y., Laurance, S., Laurance, W.F., Lawes, M.J., Amaral, I.L.d., Letcher, S.G., Lindsell, J., Lu, X., Mansor, A., Marjokorpi, A., Martin, E.H., Meilby, H., Melo, F.P.L., Metcalfe, D.J., Medjibe, V.P., Metzger, J.P., Millet, J., Mohandass, D., Montero, J.C., de Morisson Valeriano, M., Mugerwa, B., Nagamasu, H., Nilus, R., Ochoa-Gaona, S., Onrizal, Page, N., Parolin, P., Parren, M., Parthasarathy, N., Paudel, E., Permana, A., Piedade, M.T.F., Pitman, N.C.A., Poorter, L., Poulsen, A.D., Poulsen, J., Powers, J., Prasad, R.C., Puyravaud, J.-P., Razafimahaimodison, J.-C., Reitsma, J., dos Santos, J.R., Roberto Spironello, W., Romero-Saltos, H., Rovero, F., Rozak, A.H., Ruokolainen, K., Rutishauser, E., Saiter, F., Saner, P., Santos, B.A., Santos, F., Sarker, S.K., Satdichanh, M., Schmitt, C.B., Schngart, J., Schulze, M., Suganuma, M.S., Sheil, D., da Silva Pinheiro, E., Sist, P., Stevart, T., Sukumar, R., Sun, I.-F., Sunderland, T., Suresh, H.S., Suzuki, E., Tabarelli, M., Tang, J., Targhetta, I., Theilade, I., Thomas, D.W., Tchouto, P., Hurtado, J., Valencia, R., van Valkenburg, J.L.C.H., Van Do, T., Vasquez, R., Verbeeck, H., 2015. An estimate of the number of tropical tree species. Proc. Natl. Acad. Sci. 112, 7472–7477.

I.V. I. Solutions, ITT Visual Information Solutions, 2009. Atmospheric correction module: QUAC and FLAASH user's guide. Version 4.7. ITT Visual Information Solutions, Boulder, CO.

Stanley R Sternberg and CytoSystems Corporation, 1983. Biomedical image processing. IEEE Comput.

Steinwart, I., Thomann, P., 2017. liquidSVM: A fast and versatile svm package. Available from: ArXiv e-prints < 1702.06899 > .

ter Steege, H., Pitman, N., Sabatier, D., Baraloto, C., Salomão, R., Guevara, J., Phillips, O., Castilho, C., Magnusson, W., Molino, J., Monteagudo, A., Núñez Vargas, P., Montero, J., Feldpausch, T., Coronado, E., Killeen, T., Mostacedo, B., Vasquez, R., Assis, R., Terborgh, J., Wittmann, F., Andrade, A., Laurance, W., Laurance, S., Marimon, B., Marimon, B., Guimarães Vieira, I., Amaral, I., Brienen, R., Castellanos, H., Cárdenas López, D., Duivenvoorden, J., Mogollón, H., Matos, F., Dávila, N., García-Villacorta, R., Stevenson Diaz, P., Costa, F., Emilio, T., Levis, C., Schietti, J., Souza, P., Alonso, A., Dallmeier, F., Montoya, A., Fernandez Piedade, M., Araujo-Murakami, A., Arroyo, L., Gribel, R., Fine, P., Peres, C., Toledo, M., Aymard C, G., Baker, T., Cerón, C., Engel, J., Henkel, T., Maas, P., Petronelli, P., Stropp, J., Zartman, C., Daly, D., Neill, D., Silveira, M., Paredes, M., Chave, J., Lima Filho, D., Jørgensen, P., Fuentes, A., Schöngart, J., Cornejo Valverde, F., Di Fiore, A., Jimenez, E., Peñuela Mora, M., Phillips, J., Rivas, G., van Andel, T., von Hildebrand, P., Hoffman, B., Zent, E., Malhi, Y., Prieto, A., Rudas, A., Ruschel, A., Silva, N., Vos, V., Zent, S., Oliveira, A., Schutz, A., Gonzales, T., Trindade Nascimento, M., Ramirez-Angulo, H., Sierra, R., Tirado, M., Umaña Medina, M., van der Heijden, G., Vela, C., Vilanova Torre, E., Vriesendorp, C., Wang, O., Young, K., Baider, C., Balslev, H., Ferreira, I., Torres-Lezama, A., Urrego Giraldo, L., Zagt, R., Alexiades, M., Hernandez, L., Huamantupa-Chuquimaco, I., Milliken, W., Palacios Cuenca, W., Pauletto, D., Valderrama Sandoval, E., Valenzuela Gamarra, L., Dexter, K., Feeley, K., Lopez-Gonzalez, G., Silman, M., 2013. Hyperdominance in the Amazonian tree flora. Science 342, 1243092.

Tochon, G., Fret, J., Valero, S., Martin, R., Knapp, D., Salembier, P., Chanussot, J., Asner, G., 2015. On the use of binary partition trees for the tree crown segmentation of tropical rainforest hyperspectral images. Remote Sens. Environ. 159, 318–331.

United Nations, 2005. Millennium Ecosystem Assessment. Ecosystems and Human Well-being: Synthesis. Island Press, Washington, DC..

Vaglio Laurin, G., Chan, J. C.-W., Chen, Q., Lindsell, J.A., Coomes, D.A., Guerriero, L., Frate, F.D., Miglietta, F., Valentini, R., 2014. Biodiversity mapping in a tropical west african forest with airborne hyperspectral data. PLOS ONE 9, 1–10.

Vapnik, V.N., 1995. The Nature of Statistical Learning Theory. Springer-Verlag New York, Inc., New York, NY, USA.

Vaughan, C., Ramírez, O., Herrera, G., Guries, R., 2007. Spatial ecology and conservation of two sloth species in a cacao landscape in limón, costa rica. Biodiver. Conserv. 16, 2293–2310.

Warner, T.A., McGraw, J.B., Landenberger, R., 2006. Segmentation and classification of high resolution imagery for mapping individual species in a closed canopy, deciduous forest. Sci. China Ser. E: Technol. Sci. 49, 128–139.

Waser, L.T., Kchler, M., Jtte, K., Stampfer, T., 2014. Evaluating the potential of world-view-2 data to classify tree species and different levels of ash mortality. Remote Sens. 6, 4515–4545.